Miner Deposita (2006) 40: 828–848
DOI 10.1007/s00126-005-0034-6

ARTICLE

Marina A. Yudovskaya · Vadim V. Distler · Ilya V. Chaplygin · Andrew V. Mokhov · Nikolai V. Trubkin · Sonya A. Gorbacheva

Gaseous transport and deposition of gold in magmatic fluid: evidence from the active Kudryavy volcano, Kurile Islands

Received: 24 April 2005 / Accepted: 31 October 2005 / Published online: 1 February 2006

Abstract The distribution of gold in high-temperature fumarole gases of the Kudryavy volcano (Kurile Islands) was measured for gas, gas condensate, natural fumarolic sublimates, and precipitates in silica tubes from vents with outlet temperatures ranging from 380 to 870°C. Gold abundance in condensates ranges from 0.3 to 2.4 ppb, which is significantly lower than the abundances of transition metals. Gold contents in zoned precipitates from silica tubes increase gradually with a decrease in temperature to a maximum of 8 ppm in the oxychloride zone at a temperature of approximately 300°C. Total Au content in moderate-temperature sulfide and oxychloride zones is mainly a result of Au inclusions in the abundant Fe–Cu and Zn sulfide minerals as determined by instrumental neutron activation analysis. Most Au occurs as a Cu–Au–Ag triple alloy. Single grains of native gold and binary Au–Ag alloys were also identified among sublimates, but aggregates and crystals of Cu–Au–Ag alloy were found in all fumarolic fields, both in silica tube precipitates and in natural fumarolic crusts. Although the Au triple alloy is homogeneous on the scale of microns and has a composition close to $(Cu,Ni,Zn)_3(Au,Ag)_2$, transmission electron microscopy (TEM) shows that these alloy solid solutions consist of monocrystal domains of Au–Ag, Au–Cu, and possibly Cu_2O. Gold occurs in oxide assemblages due to the decomposition of its halogenide complexes under high-temperature conditions (650–870°C). In lower temperature zones (<650°C), Au behavior is related to sulfur compounds whose evolution is strongly controlled by redox state. Other minerals that formed from gas transport and precipitation at Kudryavy volcano include garnet, aegirine, diopside, magnetite, anhydrite, molybdenite, multivalent molybdenum oxides (molybdite, tugarinovite, and ilsemannite), powellite, scheelite, wolframite, Na–K chlorides, pyrrhotite, wurtzite, greenockite, pyrite, galena, cubanite, rare native metals (including Fe, Cr, Mo, Sn, Ag, and Al), Cu–Zn–Fe–In sulfides, In-bearing Pb–Bi sulfosalts, cannizzarite, rheniite, cadmoindite, and kudriavite. Although most of these minerals are fine-grained, they are strongly idiomorphic with textures such as gas channels and lamellar, banded, skeletal, and dendrite-like crystals, characteristic of precipitation from a gas phase. The identified textures and mineral assemblages at Kudryavy volcano can be used to interpret geochemical origins of both ancient and modern ore deposits, particularly gold-rich porphyry and related epithermal systems.

Keywords Gold · Cu–Au–Ag alloy · Gas transport · Kudryavy volcano

Editorial handling: N. White

M. A. Yudovskaya (✉) · V. V. Distler · I. V. Chaplygin · A. V. Mokhov · N. V. Trubkin · S. A. Gorbacheva
Institute of Geology of Ore Deposits,
Mineralogy, Petrography and Geochemistry,
Russian Academy of Sciences (IGEM RAS),
Staromonetny 35,
119017 Moscow, Russia
e-mail: maiya@igem.ru
Fax: +7-095-2302971

Introduction

The active fumarolic system of Kudryavy volcano (Iturup Island, Russia) is known for its transport and deposition of a number of ore-forming metals (Znamensky et al. 1993; Taran et al. 1995; Korzhinsky et al. 1996; Fischer et al. 1998; Tkachenko et al. 1999; Churakov et al. 2000). One of the amazing features of Kudryavy fluid discharges is the presence of mineralization, including major Mo, Re, Bi, Pb, Zn, In, and Cd, and subordinate Au and PGE, over a wide temperature range from magmatic to low-temperature epithermal.

The majority of Au in porphyry systems appears to form during the high-temperature stages of mineralization (600–700°C) as a solid solution in mainly Cu–Fe sulfides (Sillitoe 2000; Kesler et al. 2002). Experimental data also confirm that high-temperature supercritical fluids are capable of transporting significant amounts of Au in comparison to later-stage low-temperature aqueous fluids of the same magmatic hydrothermal system (Gammons and Williams-Jones 1997; Cygan and Candela 1995). However,

the Au-transporting capability of the high-temperature fluids can be difficult to constrain due to complex anionic compositions of fluids in experiments and uncertainties in the thermodynamic data. The concentration of metals in high-temperature magmatic fluids also can be underestimated in direct geological measurements such as fluid inclusions due to the typical overprinting of later hydrothermal mineralization on earlier high-temperature parageneses (e.g., Seedorff and Einaudi 2004).

In contrast, direct evidence of the capacity of magmatic vapors to transport significant quantities of metals comes from studies of active volcanoes (Taran et al. 2000), and furthermore, these fluids are thought to be analogous to those in ore-forming environments. Long-term (2001–2004) systematic observations with special attention to mineral-phase compositions and phase relationships at Kudryavy volcano have furthered our understanding of the high-temperature processes involved in forming Au mineralization.

Geological situation

About 40 active volcanoes are located in the Kurile Island Arc, which stretches from Japan to Kamchatka (Fig. 1). Kudryavy volcano is one of the youngest volcanic cones that occur in a lineament zone within the Late Pleistocene Medvezhya caldera (Fig. 2). This caldera was formed as a result of roof subsidence above the magmatic chamber during explosive activity, resulting in eruption of acid pumice, ash, and ignimbrite. Postcaldera activity consisted of successive dacitic and rhyodacitic extrusions followed by the formation of a chain of andesitic and andesite-basaltic volcanoes. The most recent lava flow of the Kudryavy volcano was in 1883, and it was composed of andesitic basalt with phenocrysts of plagioclase, olivine, and pyroxene. Persistent emissions of high-temperature fumarolic gases with occasional phreatic explosions have continued for the past 100 years. The Japanese sulfur mine built at the top of the volcano in the beginning of twentieth century is evidence for the accumulation of significant native sulfur in the fumarolic fields by that time.

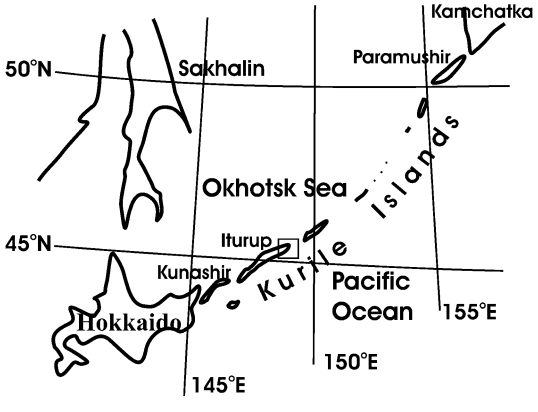

Fig. 1 Location of the Kurile Islands and Kudryavy volcano on Iturup Island. The *rectangle* marks the study area

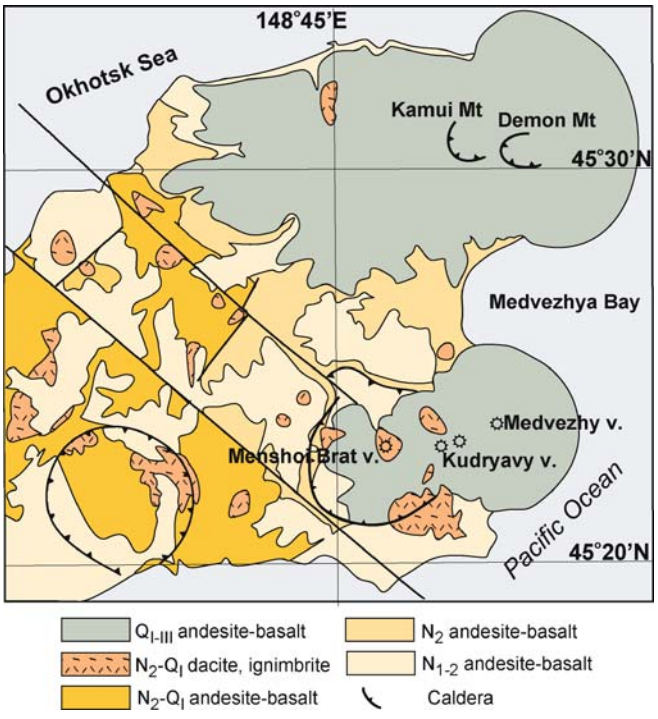

Fig. 2 Geological map of the northern part of Iturup Island (simplified from Kovtunovich et al. 2000)

Petrological studies of the volcanic rocks and xenoliths in the recent lava flows and data on melt inclusions (Tolstykh et al. 1997; Ermakov and Steinberg 1998) revealed the essential role of hybridization or contamination by crustal material in the formation of dacitic lavas. According to melt inclusion studies (Tolstykh et al. 1997), three initial melt compositions were distinguished: a basaltic melt with a homogenization temperature of more than 1,160°C, a dacitic melt with a temperature of 1,160–1,190°C, and a dacitic melt with a temperature ranging from 1,070 to 1,180°C. The source of the youngest basaltic lavas of the Kudryavy volcano seems to be a primitive melt depleted in rare earth and trace elements. The nature of the magma associated with present-day degassing is unknown. The fumarolic vents that are the sites of high-temperature discharges are confined to fractures and faults related to an andesitic extrusion exposed in the center of the eastern crater. Although the western crater appears to be the source of the youngest lava flows, only low-temperature fumarolic vents are active there. The sequence of volcanic development from dacite through andesite to basalt may be caused by both the existence of several magmatic chambers and periodic input of high-heat basaltic magma, as suggested for Baransky volcano (Bindeman 1997). The temperature of shallow degassing magma was estimated by Botcharnikov et al. (2003) to be approximately 1,050°C, which corresponds to the melt temperature of the andesitic magma. Calculations of heat balance have shown that the modern magma chamber may be less than 100 m beneath the surface, based on the assumption that the hottest temperature is located above the apex of the magmatic body.

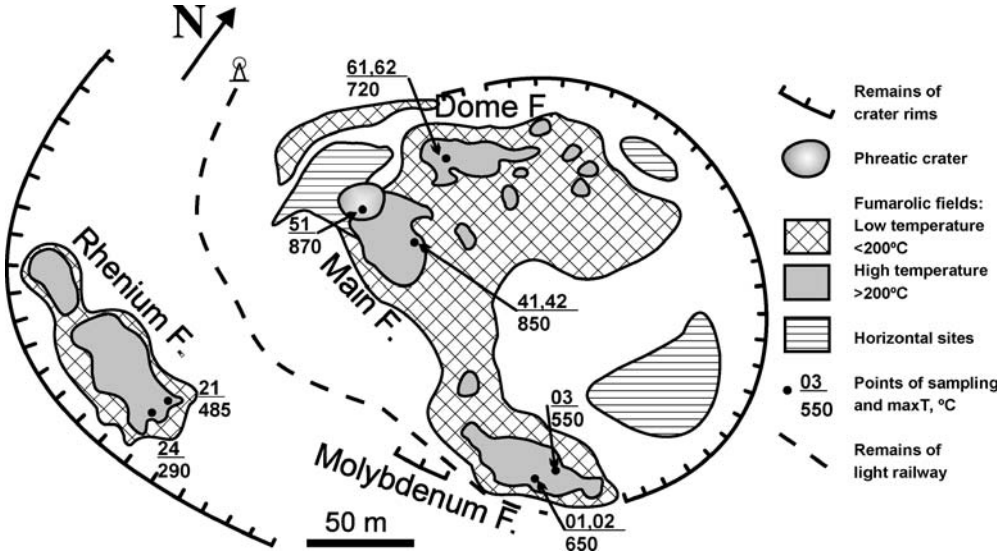

Fig. 3 Location of fumarolic fields on the top of the Kudryavy volcano (V. Znamensky, unpublished data)

Fumarolic fields

Several high-temperature fields have been distinguished in the eastern crater area on the basis of metal occurrences and temperature (Fig. 3). The main field located on a sloped andesitic dome has the highest discharge temperatures and is associated with a network of subvertical fractures and channels, the largest of which is exposed at the bottom of the youngest phreatic crater formed during the 1999 eruption. The size of this channel originally reached 3×5 m, but it has decreased in size with each successive year (Fig. 4). The highest discharge temperature measured in 2001 is 870°C, but this is lower than the maximum temperature of 940°C measured before the phreatic eruption in 1992 (Korzhinsky et al. 1996). The dome fumarole field is adjacent to the main field and is within the limits of the andesitic dome, but the discharge temperature is lower, less than 725°C. The molybdenum field and the rhenium field, both with maximum discharge temperatures of 650°C, are located on the crater rim. All high-temperature fields are bordered by a thick crust of native sulfur.

Fig. 4 The highest temperature vent (point 51, 870°C) in the bottom of the youngest phreatic crater (photo from 2001). The burning hot gas is glowing red

The fumarolic fields are distinguished on the basis of gas chemistry, mineral deposits around and inside vents, and discharge temperatures. Magnetite encrusted by fine platy crystals of molybdenite with aegirine and Na–K chlorides is a typical feature of the high-temperature cavities of the main field. High-temperature zones in the cavities on the dome and fracture fields are also filled by molybdenite in association with aegirine, garnet, and chlorides, but sulfide assemblages composed of multicolored wurtzite, Cu–Zn–Fe–In sulfides, pyrite, Cd-, In-bearing Pb–Bi sulfosalts, and late pyrrhotite are more abundant than in the main field. The molybdenum field has lower temperature gas vents and magnetite–molybdenite assemblages, which are succeeded not by sulfides but mainly by an oxide association of powellite, multivalent molybdenum oxides (molybdite-MoO_3 and tugarinovite-MoO_2), and complex sulfates. The surface of this field is covered with blue-green encrustations containing ilsemannite ($Mo_3O_8{\cdot}nH_2O$). In the rhenium field, cannizzarite ($Pb_4Bi_6S_{13}$), wurtzite, greenockite, garnet, diopside, and pyrite are widespread. In addition, there are local occurrences of rhenium sulfide (ReS_2), rheniite (Znamensky et al. 2005), and two new mineral species of rare metals [cadmoindite $CdIn_2S_4$ and kudriavite (Cd,Pb) Bi_2S_4] in this fumarolic field (Chaplygin et al. 2004).

Samples and analytical methods

Four types of material were systematically collected from the different gas vents at all the high-temperature fumarolic fields: gas, gas condensate, natural fumarolic sublimates, and precipitates in silica tubes. Experiments with mineral precipitates in the silica tubes were carried out according to the methods of Le Guern and Bernard (1982), Symonds (1993), and Korzhinsky et al. (1996). One-meter-long quartz tubes with diameters of 3–5 cm were inserted into the high-temperature vents (up to 870°C at the outlet) for a

period of 1–5 weeks. Temperature gradients depended on the inclinations of the tubes in the vent and the depths of insertion. Natural sublimates were collected near these vents from a depth of down to 1 m. The gases were collected in evacuated flasks containing an alkaline solution of KOH and Cd acetate to absorb the gas species and sulfur (Giggenbach 1975). Gas condensates were also collected from the same vents by cooling the gas with ice and water in a glass condenser. The temperature of the fluids was measured in the exit and entry points of each tube with a thermocouple to estimate the temperature gradient, assumed to be linear along the length of the tube (Korzhinsky et al. 1996).

Mineral precipitates on the walls of quartz tubes were studied directly on the glass with a scanning electron microscope (SEM; JSM-5300) with an energy-dispersive spectrometer (EDS) Link-10000 detector. They also were analyzed without carbon coating, using a low-vacuum SEM (JSM 5620) with EDS (JED-2300) at the Belov Laboratory of Crystallochemistry of IGEM RAS (Moscow). A small part of the natural sublimates, as well as the heavy separates after dissolution in distilled water and washing in heavy liquid, were put on carbonaceous tape for study by SEM. Dissolution and heavy-liquid washing is necessary for studying ore minerals, which occur as inclusions inside of massive crusts of soluble and insoluble halides, sulfates, and native sulfur. A few mineral phases were identified using a transmission electron microscope (TEM; JEM-100C) and a diffractometer (Rigaku D/Max2200). To obtain lattice parameters by TEM, the opaque mineral grains were mechanically rolled out to make the phases on the foil edges electronically transparent.

The concentrations of Au and other metals in the natural sublimate samples, in silica tube sublimates over 10-cm intervals, and handpicked mineral separates, were determined by instrumental neutron activation analysis (INAA) also at IGEM RAS. The anionic concentrations of the condensates were determined by ion chromatograph.

Concentrations of the major cations in the gas condensate samples were determined by inductively coupled plasma–mass spectrometry (ICP-MS) at the Laboratory of Analytical Chemistry, IGEM RAS. Determination of Au and other trace elements was carried out using three different methods of sample preparation and acid decomposition to avoid possible loss during analysis.

In the first method (I), gravimetric settling of the colloidal sulfur produced transparent solutions, which were then analyzed by a mass spectrometer with the addition of an internal standard. In the second method (II), 5-ml aliquots of solution were placed in silica glasses with 2 ml of concentrated HNO_3 and then boiled down to a volume of 2–3 ml to coagulate the sulfur into coarse particles. Concentrated hydrochloric acid was then added to remove the sulfur, and the solutions were subsequently heated and vaporized with repeated addition of concentrated HNO_3. The residues obtained were dried and twice water-washed then combined with 5% -HNO_3. Finally, 1-ml aliquots were diluted to 10 ml by acid for ICP-MS determination with the addition of an internal standard.

In the third method (III), solutions were placed in silica glasses, 4 ml of concentrated HNO_3 was added, and the samples were boiled down to reduce the volume to 7–8 ml. The coagulated sulfur was filtered out, and the transparent solutions were analyzed with the addition of an internal standard. The filtrates were placed in the same quartz crucible in which the coagulation was carried out and dried in an oven. The residue was diluted by concentrated HNO_3 and water, then the solutions were diluted by 2% HNO_3, and an internal standard was added for ICP-MS determination. Detection limits for the ICP-MS were (micrograms per liter) V, Cr-1, Mn-2; Co, Ni, Cu, Zn, Ga, Ge, Mo, Ag, Cd, Sn, Sb-1, I-5, Re-0.5, Au-0.2, Hg-2, TI, Pb-1, Bi-2; Pt, Pd, Os, Ir, and Ru-1 (not detected in the analyzed samples).

Metal contents in gas condensates

The minerals found in fumaroles were formed directly from gases consisting mainly of H_2O (more than 94 mol%), approximately 2 mol% of C and S compounds, 0.8 mol% HCl, and up to 1.6 mol% H_2 (Taran et al. 1995; Korzhinsky et al. 1996). The calculated oxygen fugacity was near the nickel–nickel oxide (NNO) buffer within the temperature range of 650–1,100°C and passes into the hematite–magnetite (HM) field with cooling. The major anions in the condensates are SO_4^{2-}, F^-, Cl^-, Br^-, and NO_3^-, with thio- and polysulfates also present (Table 1). The highest concentration of SO_4^{2-} (up to 12,700 mg/l) and Cl^- (up to 11,500 mg/l) occur in the highest temperature samples, and their abundances are lower in the lower temperature samples with an increase in F^- and Br^-. Maximum I^- content (8 ppm by ICP-MS data, Table 2) was found in a condensate sampled at 650°C.

The real metal contents in volcanic gases can be estimated from analysis of the gas condensates and the alkaline solutions in the gas flasks (e.g., Fischer et al. 1998), although uncondensed and water-insoluble volatile compounds can be lost during the first type of sampling. Prior to the present study, published ICP-MS analyses of the high-temperature volcanic gases (Taran et al. 2000) indicate that Au was commonly at or below the detection limit (about 1 ppb). Gold abundance in the gas condensates of the Kudryavy volcano also was initially determined

Table 1 Anionic compositions of gas condensates (milligrams per liter) determined by liquid chromatography

Sample	Date	T°C	SO_4^{2-}	F^-	Cl^-	Br^-	NO_3^-
41	August 2001	850	11,000	2.6	11,500	3.5	4.2
02	–	650	2,464	26.5	1,802	7.3	2.2
61	–	710	12,700	1.0	10,500	4.0	1.2

Table 2 Element concentrations (micrograms per liter) of gas condensates analyzed by ICP-MS

	Analytical method																			
	Method I					Method II					Method III					Filtrates				
	01	02	21	42	61	1	2	3	4	5	1[a]	2[a]	3[a]	4[a]	5[a]	1_f	2_f	3_f	4_f	5_f
Date	11/08	10/08	12/08	27/08	19/08	30/08	21/09	23/09	04/10	05/10	30/08	21/09	23/09	04/10	05/10					
V	ND	ND	9	36	47	ND	ND	ND	ND	ND	278	714	ND	214	449	ND	ND	ND	ND	ND
Cr	33	15	ND	65	22	1,212	ND	ND	ND	ND	1,095	1	ND	ND	ND	514	288	231	99	384
Mn	11	21	1	59	9	523	128	ND	ND	ND	481	30	ND	ND	ND	347	145	116	67	374
Co	1	1	ND	ND	ND	2	4	3	4	ND	4	ND	ND	ND	ND	10	7	1	3	6
Ni	24	16	16	63	2	771	351	293	156	ND	409	126	43	31	ND	255	232	358	131	287
Cu	31	14	ND	9	22	760	451	366	289	201	640	505	469	503	537	681	326	392	166	312
Zn	132	295	51	1,524	747	1,760	539	827	2,764	922	1,987	1,240	410	1,875	1,175	2,953	3,045	44.9	696	2,401
Ga	2	1	ND	1	1	3	3	1	1	ND	2	ND	1	ND	1	ND	ND	ND	ND	ND
Ge	4	4	4	8	18	13	7	13	10	10	ND	ND	ND	ND	ND	ND	285	221	ND	452
Mo	22	29	5	58	46	94	50	56	59	38	103	62	59	36	38	67	26	33	37	29
Ag	ND	ND	ND	ND	ND	ND	ND	ND	ND	ND	ND	56	5	40	24	227	12	31	8	33
Cd	7	15	3	106	81	144	61	189	1,228	1,386	132	60	162	1,036	1,451	29	13	40	66	218
Sn	29	19	8	153	69	211	139	122	175	137.8	211	126	102	178	118	111	65	68	38	47
Sb	7	9	2	5	6	21	7	7	7	6	24	14	14	16	11	11	9	14	6	36
I	7,950	1,803	ND	469	4,837															
Re	0.2	ND	0.1	ND	0.2	7.9	0.7	4.4	8.8	2.2	22.5	21.4	14.4	5.1	6.1	1.4	1.2	2	0.2	1.4
Au	1.3	0.9	1.1	2.4	1.7	ND	ND	ND	ND	ND	ND	0.3	2.1	1.9	2.2	ND	0.2	ND	ND	ND
Hg	198	317	213	128	179	8	ND	33	ND	ND	90	183	152	154	158	6	3	4	8	2
Tl	16	19	2	36	46	151	71	444	366	180	79	60	226	162	141	ND	ND	ND	ND	ND
Pb	178	263	12	583	997	2,778	1,297	2,897	5,095	3,245	1,642	1,071	1,592	2,217	2,471	453	264	553	190	665
Bi	16	40	2	34	57	295	126	174	407	181	177	87	88	165	128	58	26	36	41	44

Numbers 01, 02, 21, 42, and 61 were collected in 2002 from the sample locations in Fig. 3. Numbers 1–5 were collected repeatedly from point 61 (Fig. 3) in 2003 and analyzed according to method II

Blank table entries were not analyzed

ND Not detected

[a]Same samples as numbers 1–5 but analyzed according to method III. Numbers 1_f–5_f are filtrates of these samples

(Taran et al. 1995) to be below the ICP-MS detection limit (1 ppb).

The results of the trace element determinations in gas condensates of Kudryavy volcano are given in Table 2. Gold concentrations range from 0.9 to 2.4 ppb using method I. Gold concentrations for method II are below the detection limits, but the same samples analyzed according to method III show that all measurable Au was in the solution, and its concentration ranged from 0.3 to 2.2 ppb. Similar trends are found in the results for other elements in Table 2. Rhenium contents using method I (up to 0.2 ppb) are slightly above the analytical detection limit, consistent with previously reported data (Distler et al. 2002). Condensate from the rheniite (ReS_2)-bearing vent in the rhenium field contains about 0.1 ppb of Re. Condensate from the molybdenum fields, from the vent with precipitates of Re-bearing molybdenite and K perrhenate ($KReO_4$), contains 0.2 ppb of Re.

The condensate analyses using method II yield higher contents of Re ranging from 0.7 to 8.8 ppb, and a maximum Re content of 22.5 ppb was found with method III. In this case, Re concentration abundances correlate with Mo, although a significant part of Mo was fixed in the filtrates (Table 2). Rhenium concentrations ranging from 7 to 200 ppb in Kudryavy gas condensates analyzed by the isotope dilution method (Tessalina et al. 2005) confirm that such high abundance of Re is closer to the real value than the data previously reported (Taran et al. 1995; Korzhinsky et al. 1996; Distler et al. 2002). Other elements, besides Re and Au, showed higher values using method III compared to method II. This indicates a loss during volatile formation in method II. The greatest differences in concentrations were detected for Au, Ag, Hg, V, Re, and Tl. Other groups of elements (Cu–Zn–Cd–Ge–Sn and Pb–Bi) were not lost in method III, and the corresponding filtrates are enriched in these elements. Mo, Sn, Pb, Cd, and possibly Au show a positive correlation with an increase in temperature. Mercury has an inverse relationship with temperature. Analyses over a 1-month period (Table 2, analyses 1–5) of condensates collected from the same point (720°C) on the dome field show that gas enrichment can vary significantly with time.

The mineralogy of quartz tube precipitates

Zonation of the mineral precipitates was roughly similar in all of the tubes studied, suggesting insignificant redeposition and metasomatism. Zoning of precipitates in tubes from Kudryavy volcano has been described in detail

elsewhere (Korzhinsky et al. 1996; Tkachenko et al. 1999; Churakov et al. 2000), so we will only summarize the key features of the zoning with respect to the Au distribution and Au-bearing mineral associations in the examples of tube 61 from the dome field with an outlet temperature of 720°C and tube 03 from the molybdenum field with an outlet temperature of 550°C. Additional mineralogical observation is also reported for tube 51 from the youngest crater (Fig. 4) and tube 02 from molybdenum field, with outlet temperatures of 870 and 650°C, respectively.

The hottest zone at the orifice in tube 61 (the crystobalite zone of Korzhinsky et al. 1996) is poor in mineral precipitates. Rare single crystals of magnetite, wolframite, scheelite, powellite, and complex Fe–K molybdate are characteristic for this high-temperature oxide zone (Fig. 5). Precipitates large enough for INAA occur only in the molybdenite zone at a distance of 25 cm at 720°C. This zone has a length of about 5 cm and is composed of Re-rich molybdenite (Re 2.6 wt%) with rare grains of Na–K chlorides, Fe-, Ca-, and K-molybdates, magnetite, and wolframite. It has a sharp border with the following narrow zone of Na–K chlorides composed of coarse- to fine-grained, massive K–Na chlorides usually with a yellow-red color. Sulfide minerals (pyrite, galena, and cubanite) and rare native metals (chromium and molybdenum) were found in this zone together with a few crystals of magnetite, molybdates, wolframite, and aegirine. Fine irregular-shaped particles of native Mo were detected here in an unusual association of coexisting platy molybdenite and oxidic molybdenum phases such as powellite and ferrimolybdite. The elongated crystals of native Cr have a skeletal morphology and grow together with Fe silicate and ferberite (Fig. 6a). Gold abundance in the precipitates of the molybdenite zone (1.8 ppm) is slightly lower compared to that in the Na–K chloride zone (Au 2.1 ppm), which was depleted in all other metals (Table 3, Fig. 5).

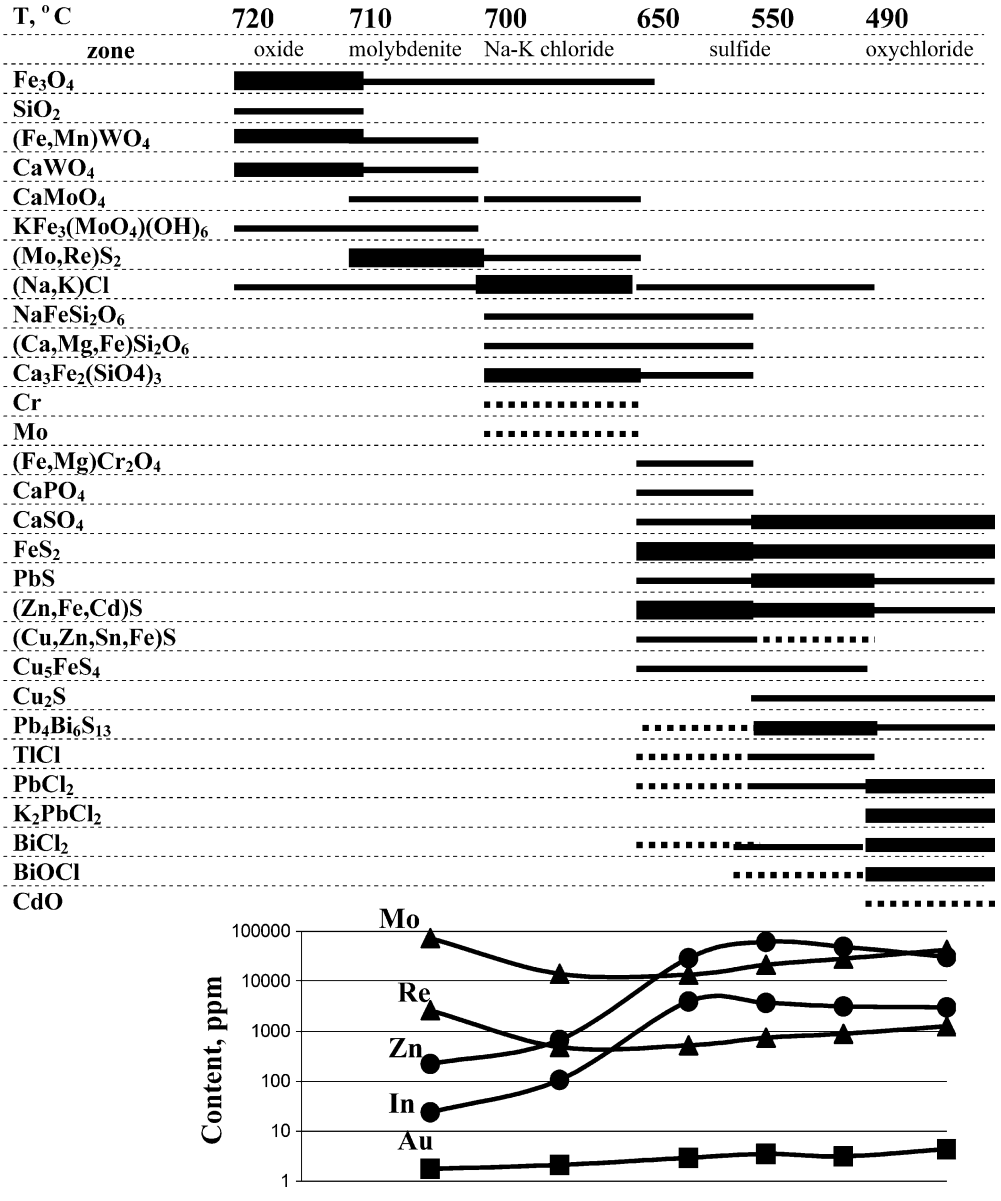

Fig. 5 Distribution of minerals and representative elements along the Kudryavy tube 61. Temperatures are given for the beginning of each analyzed interval from the hot end of the tube

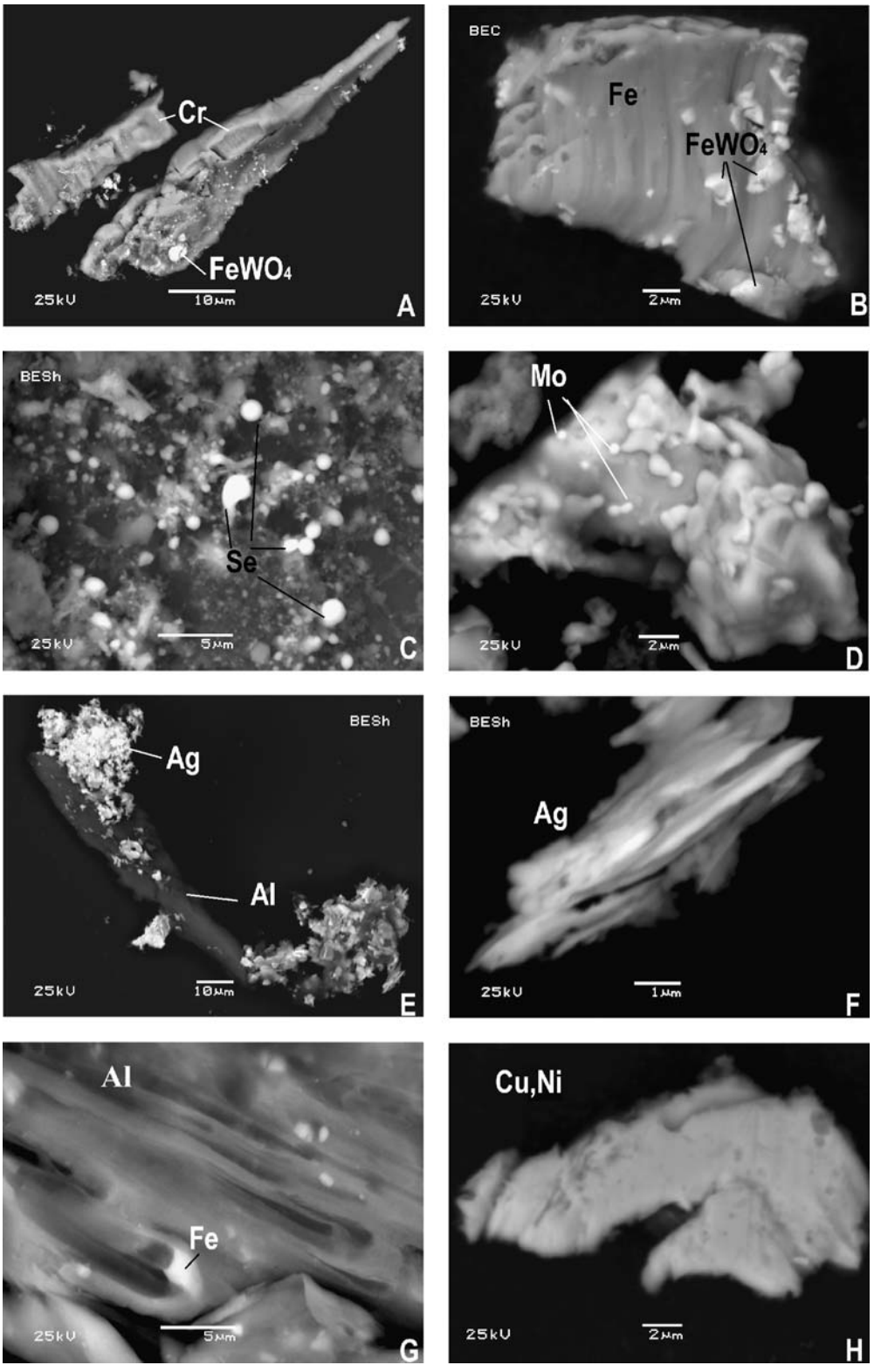

Fig. 6 Native metals in the tube precipitations of the Kudryavy fumaroles, SEM, BSE image. **a** Elongated crystals of native Cr; **b** grain of native Fe with $FeWO_4$ inclusions; **c** spherical particles of native Se among Na and K sulfates; **d** spherical particles of native Mo on the surface of Gd titanate; **e** tiny platy crystals of native Ag on the particle of native Al, with the silica glass as background; **f** detail of intergrowth of native Ag lamellae; **g** morphology of the surface of native Al with microholes; **h** particle of Cu–Ni alloy

The sulfide zone (<650°C) contains mainly Fe and base-metal sulfides. Variation of metal contents along the tube indicates the precipitation of Zn sulfides (with Cu, Cd, and In admixture) followed by pyrite, galena, and finally, Pb–Bi sulfosalts (also with In, Cd, and Mo) and sulfochlorides. Also common in this zone are magnetite, chromite, garnet, and pyroxene. Among the most distant precipitates were octahedral crystals of rare spinel, Zn-bearing herzinite intergrown with apatite (Table 4). Pb, Bi, and Tl chlorides occurred in the coolest temperature zone. The maximum

Table 3 Element concentrations in the tube precipitates by INAA

Tube	6102						0201		0303						
L (cm)[a]	25	30	40	50	60	80	80	100	30	40	50	60	70	80	90
T (°C)[b]	720	710	650	600	550	490	450	400	560	550	450	400	350	300	250
Na_2O (wt%)	21.73	28.91	17.4	18.43	14.83	14.38	14.01	7.77	34.81	22.89	21.29	24.64	2.44	4.5	3.39
CaO (wt%)	ND	ND	ND	5.8	21.6	ND	24.6	7.9	ND	ND	ND	15	45.8	ND	ND
Fe (wt%)	1.08	1.74	4.21	3.49	3.49	3.29	7.07	8.78	2.02	1.99	2.78	3.81	2.95	5.9	2.53
Sc (ppm)	0.9	0.6	1.5	2.3	0.5	0.6	0.5	ND	4	1.2	10.4	5.9	ND	ND	0.7
Cr (ppm)	63.1	12.2	101.9	73.5	691.8	161	113.6	93.5	18.9	36.9	13.4	ND	ND	142.1	62.3
Zn (ppm)	222	678	29,220	62,032	49,197	30,629	39,447	87,328	1,223	28,378	31,802	68,749	69,742	19,420	14,381
As (ppm)	ND	ND	233	282	429	4,348	2,050	3,161	ND	273	424	809	4,345	26,785	124,344
Se (ppm)	32.8	10	53.5	98.7	238.3	248.1	529.9	974.8	39	81.6	368.7	2,326.7	3,069.7	2,827.7	5,454.7
Br (ppm)							1,175	765	948	907	1,040	1,426	1,357	3,117	3,697
Mo (ppm)	72,366	14,076	13,546	21,429	28,291	42,537	53,290	63,890	19,340	9,344	13,370	8,576	20,370	59,560	38,800
Ag (ppm)	17.8	36.4	94.3	76.8	83	104.1	88.9	140	42.9	45.3	39.9	29.5	65.8	148.3	113.1
Cd (ppm)	ND	101	6,809	8,514	6,124	3,656	3,671	9,516	452	5,968	6,222	10,673	9,716	3,041	3,981
In (ppm)	24	106	3,926	3,696	3,136	3,023	6,033	7,658	521	3,643	3,372	5,280	5,736	4,380	2,808
Sb (ppm)	ND	ND	2.2	6.9	14	42.5	16	24	1	1	5	46	172	212	296
Cs (ppm)	1.4	4.3	119.2	330.7	692.6	902.3	38.4	82.5	6	22.5	97.3	798.7	456.1	298.3	223.1
W (ppm)	ND	218	438	509	468	512	3,067	2,157	972	800	884	1,254	994	1,264	1,002
Re (ppm)	2,643	487	526	746	887	1,257	964	1,214	218	124	97	48	284	1,101	727
Au (ppm)	1.77	2.13	2.95	3.51	3.15	4.40	2.98	5.53	2.04	1.75	1.01	1.25	1.76	8.12	4.59

Blank table entries were not analyzed
ND Not detected
[a]Distance from the hottest end of the tube
[b]Approximate temperature (sample locations are in Fig. 3)

Au content of 4.4 ppm was detected in the oxychloride zone at the end of this tube at 490°C (Table 3, Fig. 5). Fine-grained and dispersed precipitates of anhydrite, metal chlorides, complex salts, and oxychlorides such as bismoclite were common in this zone.

In tube 03, the high-temperature molybdenite zone was absent as expected. The common oxidic phases (magnetite, wolframite, and silicates) of the hotter Na–K chloride zone were replaced by various sulfide minerals in the sulfide zone with cooling (Fig. 7). Further up the tube, anhydrite, Pb and Bi chlorides, and bismoclite were common in the oxychloride zone with subordinate amounts of Zn–Cd–Fe–In sulfides. Thallium, Bi, and Cu iodides, K–Cd chloride, Cd–In chloride, K–Pb chloride, and sulfate, were also widespread. The oxychloride zone was followed by a zone of native sulfur at about 250°C.

Gold abundances were uniform along the hotter length of tube 03 in the range of 1–2 ppm (Table 3); only the oxychloride zone was enriched in Au (up to 8 ppm). The oxychloride zone (the last 10-cm interval on the cool end of the tube with approximate temperature of 400°C) in tube 02 also is enriched in Au, up to 5 ppm (Table 3). Silver,

Table 4 Chemical compositions (wt%) of spinels in the fumarole precipitations by EDS

No.	Sample	MgO	Al_2O_3	TiO_2	Cr_2O_3	FeO	Fe_2O_3	∑
1[a]	02	1.86	7.43	4.54	23.73	34.34	28.92	100.81
2[a]	02	2.62	7.67	6.28	29.93	34.75	19.02	100.27
3[a]	02	3.53	8.19	6.25	31.90	34.51	19.26	103.64
4[a]	02	2.20	7.05	7.14	28.40	36.59	20.55	101.93
5[b]	61	11.20	55.99	1.43	–	22.19	0.12	94.14
6[c]	67	9.04	7.88	–	55.97	18.95	7.34	99.48
7[d,e]		14.53	23	0.39	39.56	22.06	0.11	99.65
8[d,f]		13.44	28.99	0.44	29.1	27.57	0.31	99.94

[a]Chromian spinel in the tube sublimates (*T*=620°C)
[b]Herzinite in the tube sublimates (*T*=600°C) (with 2.54 wt% ZnO)
[c]Chromite in the natural encrustation (*T*=620°C) (with 0.31 wt% MnO)
[d]Chromian spinel in the volcanic rocks of the Kudryavy volcano
[e]By Ermakov et al. 2001 (with 0.11 wt% SiO_2, average from three analyses)
[f]By Tolstykh et al. 1997 (sample locations are in Fig. 3)

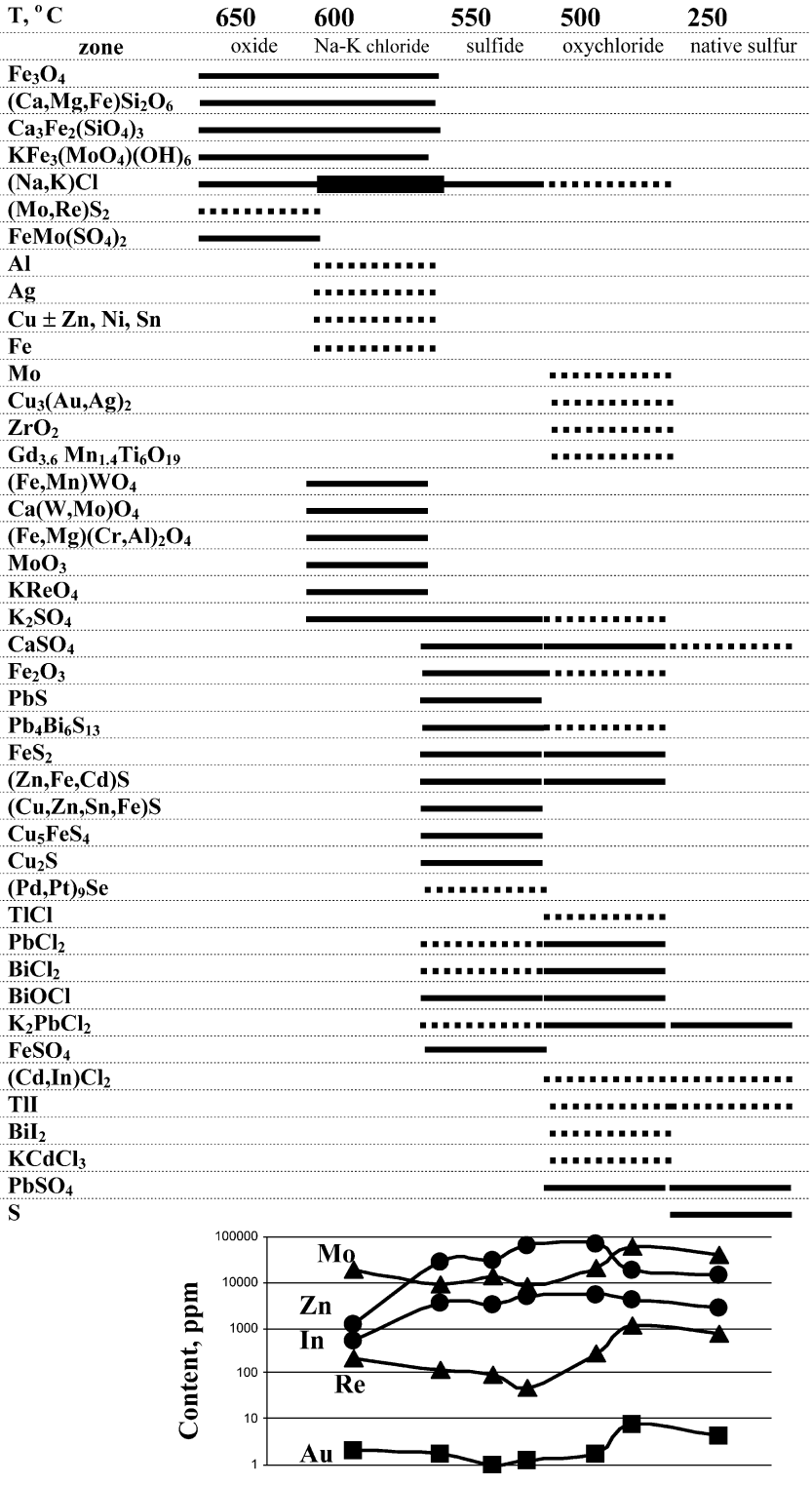

Fig. 7 Distribution of minerals and representative elements along the Kudryavy tubes 02 and 03 from the molybdenum field. Temperatures are given for the beginning of each analyzed interval from the hot end of the tube

Mo, W, and Re concentrations could not be correlated with a mineral phase from SEM observation. It is possible that W, Re, and Mo (and Au) are present in sulfochloride complexes as minor to trace components at lower temperature. As noted in a previous study (Symonds 1993), crystals from the high-temperature zones are commonly coarser in size, have a higher idiomorphism, and have a more stable chemical composition compared to those from low-temperature zones.

Our data on Au distribution in the zoned tube precipitates are consistent with previous results (Tkachenko et al. 1999), which show for the Kudryavy fumaroles that Au abundance in the tube sublimates increases with cooling to reach a maximum concentration of 4.4 ppm at approximately 260°C on the border of native sulfur precipitation.

Thus, maximum Au enrichment is observed in the oxychloride zone in the temperature range of 250–490°C.

The mineralogy of fumarolic deposits

Previous studies showed that Au contents in bulk samples of fumarolic crusts were 0.1–0.2 ppm, with a maximum value of 0.4 ppm in the rheniite-bearing sulfide concentrate from the rhenium field (Distler et al. 2002). Au enrichment was also found in wurtzite (in a cavity at 560°C) containing 5 ppm Au (Table 5). Wurtzite from Kudryavy fumaroles is commonly enriched in Fe, Cd, Cu, In, and Sn, up to the formation of a pure mineral phase of rare metals, among which greenockite is the most abundant (Kovalenker et al. 1993). Yellow translucent hexagonal plates of wurtzite were intergrown with dodecahedral grains of pyrite. INAA analysis of pyrite shows an Au content of 3.4 ppm (Table 5), but it is possible that the mineral separates were contaminated by fine particles of native gold; microbeam spot analyses would be needed to determine the actual Au content in these minerals. Magnetite from the high-temperature assemblage (720°C) contains low Au (0.3 ppm), and an Re-bearing molybdenite (1.5 wt% Re) from the cavity with a temperature of 650°C was found to be Au-free.

Gold occurrences and mineral assemblages

The most widespread mineral occurrence of Au in the Kudryavy fumaroles is Cu–Au–Ag triple alloy (Fig. 8a) in contrast to the pure native Au commonly observed in the mineral associations of other volcanic systems (Vergasova et al. 1982; Meeker et al. 1991; Fulignati and Sbrana 1998; Taran et al. 2000). Single grains of native Au and binary Au–Ag alloys only occur in minor amounts in Kudryavy fumaroles.

Commonly, alloy particles are represented by the intergrowth of lamellar crystals in which the surface is pitted with fine holes. Sometimes, intergrowths of the nano-sized crystals can be observed (Fig. 8b). The greatest abundance of Cu–Au–Ag alloy particles was found in the crust lining a fumarole cavity (690°C) on the Dome field. This cavity is next to a hotter fumarole (710°C) where tube 61 was inserted. Au alloy (Fig. 8c,d) associated with K–Na chlorides, wurtzite, pyrrhotite, Pb–Bi sulfosalts, and galena (Fig. 9) precipitated on the overhang of the fumarolic vent.

Transparent acicular aegirine ($NaFeSi_2O_6$) and skeletal-like magnetite (Fig. 9a) appear to be the earliest mineral phases in the crust lining this cavity. The main central part is composed of massive salts and bipyramidal crystals of quartz, which occurs as a paramorph of alpha-quartz on beta-quartz (Fig. 9b). There are no prismatic faces in these crystals, and all six pyramid faces have the identical growth steps that formed simultaneously, which implies they had equal growth rates as faces on the hexagonal pyramid. The step-like surface of the faces is covered with numerous irregular-shaped holes.

Hexagonal pyrrhotite ($Fe_{1-x}S$), determined by EDS and diffraction data (Fig. 9c,d), is one of the last minerals to form in the crust. It occurs as triangular plates, golden hexagonal crystals, and plate intergrowths with Na–K chlorides. Idiomorphic tabular crystals of cubanite ($CuFe_2S_3$) and a sakuraiite-like mineral [(Cu,Zn,Fe,Sn)S] (Table 6) are present but rare. Iron-poor pyrrhotite commonly contains about 3 wt% Cu as an admixture (Table 6). In addition, pentlandite [$(Fe,Ni)_9S_8$] and polydymite ($NiNi_2S_4$) were found in these assemblages.

Dodecahedral pyrite (Fig. 9e) and yellow-, brown-, and red-colored hexagonal plates of wurtzite (Fig. 9f) formed

Table 5 Element concentrations in the mineral separates. Na_2O, CaO, and Fe, wt%; all other elements, ppm

Sample	67	67	01	41
T°C	620	620	650	830
Mineral	Pyrite	Sphalerite	Molybdenite	Magnetite
Na_2O (wt%)	0.54	0.62	ND	5.75
CaO (wt%)	ND	ND	ND	1.2
Fe (wt%)	44.47	4.82	0.71	41.58
Sc (ppm)	3.4	ND	0.7	17.5
Zn (ppm)	13,216	379,402	375	718
As (ppm)	249	ND	ND	ND
Se (ppm)	414.6	353.3	380.6	ND
Br (ppm)	196	348	ND	ND
Mo (ppm)	722	ND	525,400	3,821
Ag (ppm)	69.1	335.9	ND	ND
Cd (ppm)	5,088	92,257	ND	33
In (ppm)	1,642	6,837	20	ND
Cs (ppm)	44.6	ND	ND	335
Re (ppm)	33	ND	13,746	26
Au (ppm)	3.36	4.95	ND	0.35

Sample locations are in Fig. 3
ND Not detected

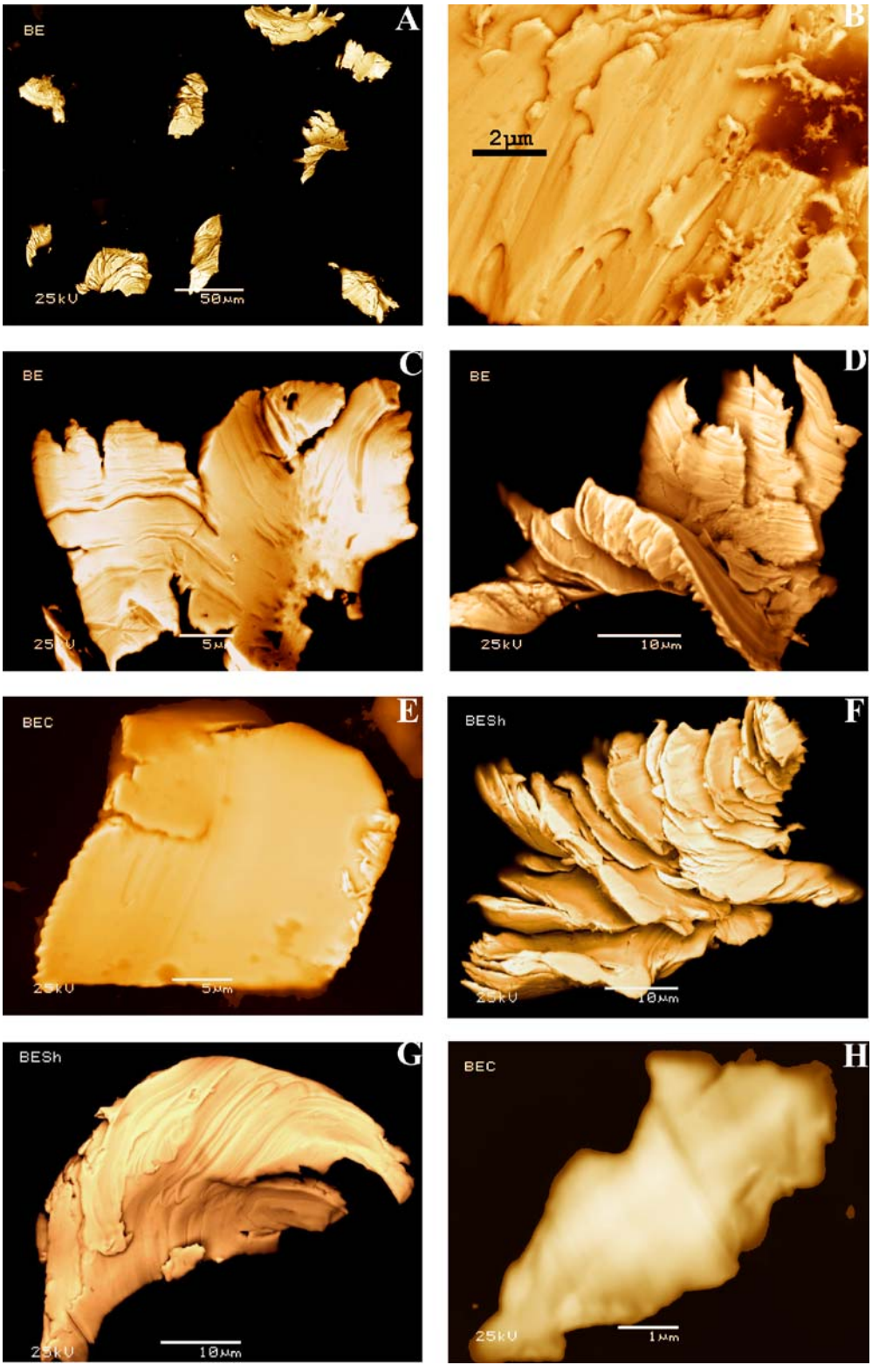

Fig. 8 Morphology of crystals and lamellar aggregates of Cu–Au–Ag triple alloy, SEM, BSE image, digital color. **a**–**d** Particles in fumarolic crust from the dome field (690°C): **a** general view; **b** details of the alloy surface with microholes and nano-sized crystals, field of view 10 μm; **c**, **d** front and backside of the different twisted aggregates; **e** plates of alloy from the silica tube precipitations in the highest temperature vent (870°C); **f**, **g** lamellar intergrowths in natural crust from the molybdenic field (650°C); **h** Au alloy particle from the rhenium field

earlier than pyrrhotite. The lower-temperature zone is encrusted with elongated platy crystals of Pb–Bi–In–Sn sulfosalt minerals together with framboidal galena (Fig. 9g), lamellar Se-bearing acanthite (Ag_2S) (Fig. 9h), acicular ikunolite [$Bi_4(S,Se)_3$], anglesite ($PbSO_4$), anhydrite ($CaSO_4$), and Na–K chlorides.

Gold alloy particles were also found in the precipitates inside tube 51 inserted into the largest fumarolic vent, with the highest gas temperature (870°C) and the highest rate of gas discharge, located at the bottom of a young phreatic crater on the main field (Fig. 4). A thin single plate of Au alloy, approximately 30 μm in size (Fig. 8e), and a helicoid

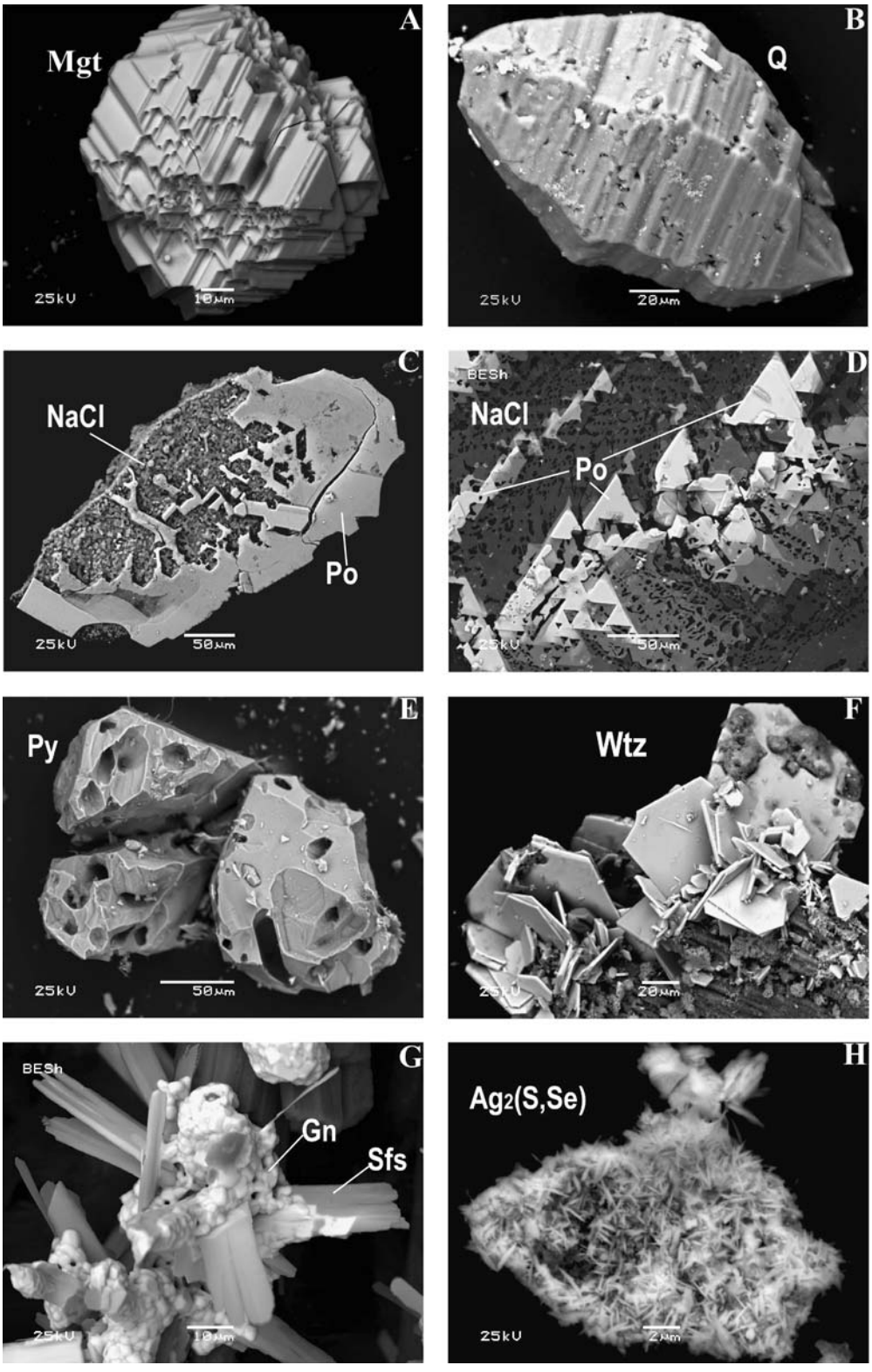

Fig. 9 Natural mineral assemblages of gold-bearing fumarolic crust from the dome field (690°C), SEM, BSE image. **a** Skelet-like octahedral magnetite (*Mgt*); **b** a paramorph of α-quartz on β-quartz (*Q*); **c** plate of hexagonal pyrrhotite (*Po*) and halite (*NaCl*); **d** detail of pyrrhotite–halite intergrowth; **e** pyrite (*Py*) from its intergrowths with chlorides; **f** incrustation of wurtzite (*Wtz*) on anhydrite and pyrite; **g** incrustations of platy Pb–Bi sulfosalts (*Sfs*) and framboidal galena (*Gn*); **h** fine lamellar acanthite $Ag_2(S,Se)$

aggregate of plates more than 200 μm were found here (Fig. 10a). These particles crystallized inside a tube exposed during a period of less than 2 weeks. The mineral association includes Na–K chlorides and different oxide compounds such as ferberite [$(Fe,Mn)WO_4$], magnetite, scheelite ($CaWO_4$), powellite ($CaMoO_4$), rutile, and hematite. It should be noted that particles of native Fe, Cu–Zn, Cu–Ni, and Fe–Cr–Ni alloys are abundant in similar high-temperature tube precipitates. The particle of native Fe from the Au-bearing assemblages contains ferberite in-

Table 6 Chemical compositions of the sulfides (wt%) in the fumarole precipitations determined by EDS

Mineral	S	Fe	Cu	Zn	Co	Ni	Sn	∑
Pyrrhotite	43.05	53.39	3.01	ND	ND	ND	ND	99.45
Pyrrhotite	39.82	57.60	1.69	ND	ND	ND	ND	99.11
Cubanite	37.89	35.75	20.12	0.52	ND	ND	2.15	96.43
Pentlandite	36.73	24.84	ND	ND	2.67	34.61	ND	98.85
Polydymite	41.43	1.92	ND	ND	ND	52.68	ND	96.03
Sakuraiite?	34.70	1.39	26.54	10.78	ND	ND	26.91	100.32
Sakuraiite?	24.60	3.74	37.59	17.15	ND	ND	17.01	100.08

ND Not detected

clusions, suggesting that is a natural precipitate and not an external contaminant. The striped surface of native Fe with numerous gas channels and holes is similar to the morphology of the Au alloys (Fig. 6b).

Galena, copper sulfide, and pyrite are rare phases occurring with more widespread sulfates of Ba, Pb, Na, and K. Occurrences of spherical particles of native Se were found in a sulfate encrustation in the same temperature zone of the silica tube (Fig. 6c). The size of spheroids ranged from less than 0.2 to 3 μm. Some K–Pb sulfates formed radial intergrowths of elongated tubular crystals and are anomalously enriched with Se, which can possibly substitute for sulfur: $K_2Pb[(S,Se)O_4]_2$. The thickness of the precipitates in this tube was insignificant and did not exceed 1 mm due to the high rate of gas discharge and minimal cooling along the length of the tube. The native elements mentioned above and all other minerals grew directly on a glass surface and lacked a salt substrate.

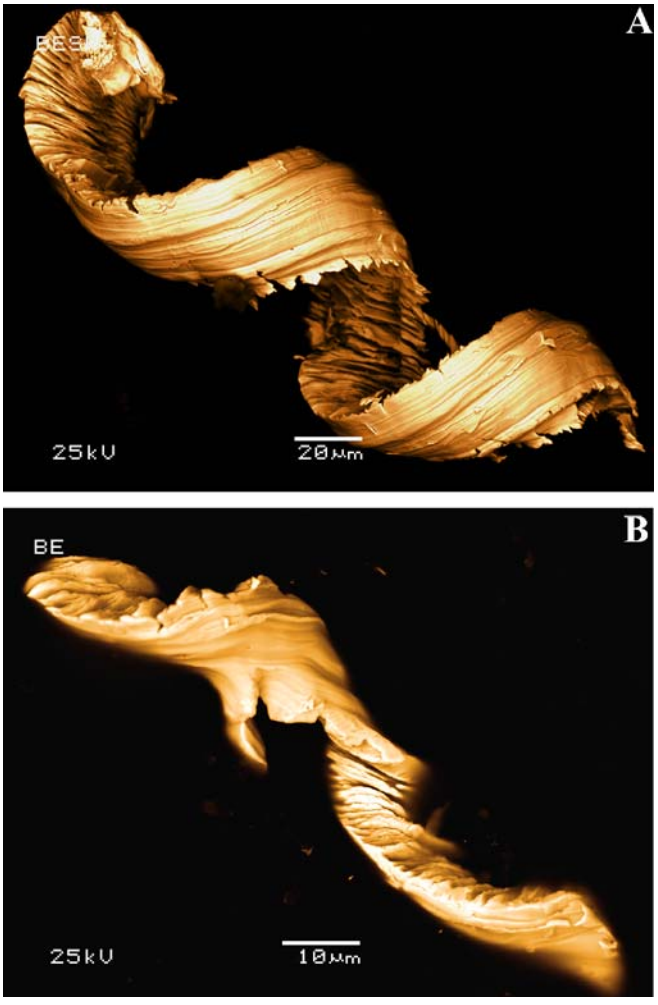

Fig. 10 Morphology of spiral-shaped aggregates of Cu–Au–Ag triple alloy, SEM, BSE image, digital color. **a** Aggregate of lamellar crystals from a silica tube (870°C, tube 51); **b** aggregate of lamellar crystals from natural fumarolic crust (710°C, point 41), the main field

A spiral-like aggregate (Fig. 10b) was found among the fumarolic deposits of the main field. This particle of a triple alloy occurred in association with molybdenite, magnetite, and Na–K chlorides in a cavity with temperatures exceeding 750°C.

Twisted aggregates of alloy plates of up to 50 μm in size (Fig. 8f,g) were found in a natural fumarolic crust from the molybdenum field. The top surface of the crust was covered by green-blue amorphous ilsemannite ($Mo_3O_8 \cdot nH_2O$) and white fine-grained anhydrite. The bottom of the overhanging part exposed to the cavity (about 650°C) is encrusted by rose-like aggregates of molybdenite flakes. Magnetite, hematite, powellite, and Na–K chlorides are common in this assemblage, and blue translucent crystals of molybdite occur inside the small cavities and fractures closer to the surface. In the same molybdenum field, Au alloy was also found in tube precipitates within an oxychloride zone with an approximate gas temperature of 450°C. This section of the tube was mainly filled with fine-grained Na–K chlorides, complex sulfates, sulfochlorides, and oxychlorides [dominated by bismoclite (BiOCl)], among which were rare crystals of wolframite, magnetite, hematite, and iodides. Hematite forms both pseudomorphs on magnetite and plate crystals. Bismoclite also occurs as plate crystals and aggregates (Fig. 11a). Native Mo in this association occurred as fine spheres of less than 2 μm in size (Fig. 6d).

The mineral composition of the high-temperature zones, which are absent in tube 03 with an outlet temperature of 550°C, can be compared to the material from another tube (tube 02) inserted into the vent with a maximum temperature of 650°C in the molybdenum field (Fig. 7). The first 50 cm of this tube was empty due to the high gas speed and absence of a temperature gradient. Only rare Ca–Fe silicates, magnetite, and complex Fe–Mo sulfate precipitated on the clear glass, which was slightly corroded by the acidic gases. Aggregates of platy crystals of native Ag, which encrusted an elongated tube-shaped particle of native Al, were found in this zone of the tube directly on

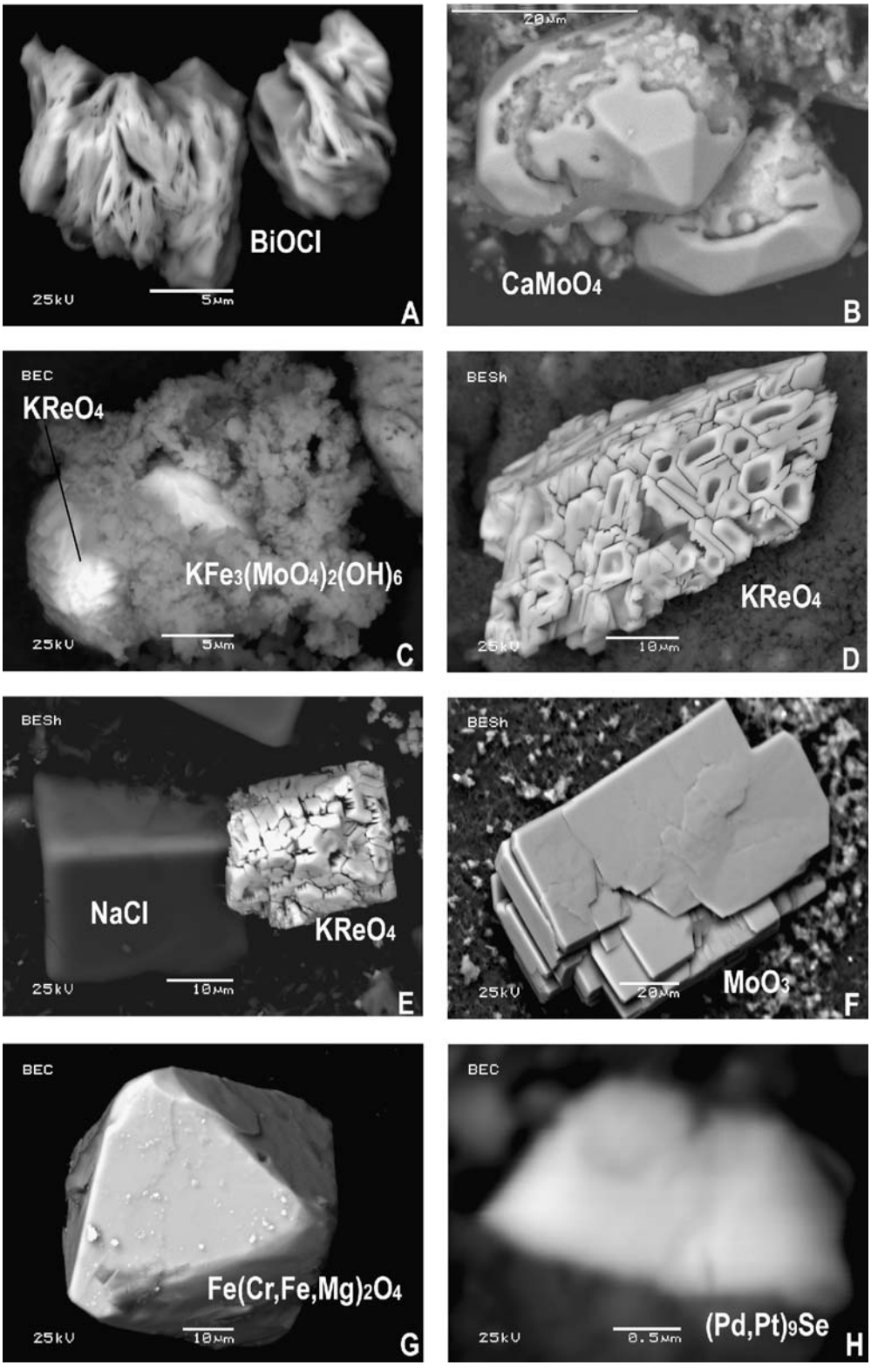

Fig. 11 Mineral assemblages of gold-bearing tube precipitations from the molybdenum field with maximum temperature of 650°C SEM, BSE image. **a** Platy crystals of bismoclite (*BiOCl*); **b** euhedral crystals of powellite ($CaMoO_4$); **c** disperse ferrimolybdite on the skeletal crystal of K-perrhenate ($KReO_4$); **d** Cluster structure of the coarse grain of K-perrhenate; **e** halite and K-perrhenate on the silica glass; **f** molybdite (MoO_3) among fine-disperse silicates and Mo-bearing complex sulfates; **g** euhedral crystal of chromium spinel; **h** tiny plate of Pd–Pt selenide $(Pd,Pt)_9Se$

the glass (Fig. 6e). Pure native Ag occurred as rose-like and irregular intergrowths of plates. The largest aggregate reached 50 μm in size, and the length of the native Al particle exceeded 50 μm. The coarser plates were intergrown; the finer plates, spheres, and icicle-like particle less than 1 μm in size are disorderly located on the surface of coarser ones (Fig. 6f). The mineral surfaces are covered with submicron-sized pores and channels (Fig. 6g). The occurrence of native Al has been described previously by Korzhinsky et al. (1996), who explained the existence of a disequilibrium association of Al, Si, and Ti by their preservation in a salt matrix. Our observations also suggest the

possibility of native metal sublimating directly in the gas within the tubes. Particles of cuprous alloys (Cu–Zn, Cu–Ni, Cu–Sn, and pure Cu) also are abundant in the tube precipitates (Fig. 6h).

Mineral associations, including abundant Na–K chlorides, K-perrhenate, Ca–Fe silicate, Fe–Mg–Al–Cr spinels, wolframite, Ca and Fe–K molybdates (Fig. 11b,c), and molybdite, occur in a zone having an approximate temperature of 600°C. Fine crystals of K-perrhenate form aggregates; the coarser ones up to 200 μm in size commonly have skeletal morphology (Fig. 11c–e). The skeletal morphology reflects fast crystallization from a low-density gas with the preferential growth of edges and tops compared to faces under the conditions of a high-speed laminar flow. Korzhinsky et al. (1996) also remarked on the occurrence of native Au crystals in association with K-perrhenate. Euhedral transparent crystals of molybdite are common in this zone (Fig. 11f). Tabular idioblasts of molybdite on the walls of the tube are similar in morphology to the natural blue crystals.

The occurrence of fine octahedral crystals of Cr spinel intergrown with other minerals implies their precipitation from gases instead of their transport as a solid phase. The Cr spinels occurring in the natural sublimates contain 55.97 wt% Cr_2O_3 (Table 4, Fig. 11g) and differ from the composition of accessory spinel in the host volcanic rocks (Cr_2O_3 from 29 to 40 wt%). Cr spinels in tube sublimates, in contrast, are characterized by low Mg, Al, and Cr contents (Table 4, analyses 1–4).

Various Cu (±Fe) sulfide minerals, including cubanite, chalcopyrite, sakuraiite, and covellite, were succeeded in a lower temperature zone by copper sulfates. Microplates of Pd–Pt selenide were identified in association with Cu sulfides, pentlandite, scheelite, and wolframite. The particles, less than 5 μm in size, contained 34 wt% Pt, 50–51.8 wt% Pd, 7–7.2 wt% Se, about 4 wt% Fe, 2 wt% Ni, and 1 wt% Cu (Fig. 11h) and correspond to the formulae $(Pd, Pt, Fe, Ni, Cu)_9Se$.

Gold minerals occur in precipitates from fumaroles and quartz tubes in association with rheniite in the rhenium field (point 21, Fig. 3). A tiny crystal of triple alloy about 7 μm in size (Fig. 8h) was detected in association with Sb-bearing native Sn, scheelite, barite, and pyrite, and was precipitated in the temperature range of 290–300°C, whereas the maximum temperature in the channel was 380°C. Among the other Au-bearing phases, the binary Au–Ag alloy corresponded to $Au_{0.84}Ag_{0.14}Cu_{0.02}$ in association with scheelite and galena, which was found in the natural crust from the rhenium field.

In addition, numerous fine submicron grains of native Au were observed in unusual mineral assemblages with rheniite. Coarse layered crystals of rheniite grew as thin trigonal plates with thicknesses of less than a tenth of a micron. Rose-like aggregates of the smaller platy molybdenite epitaxially encrusted the rheniite surface, and consistent with trigonal crystallographic directions, crossed at an angle of 120°. Gold crystals smaller than 1 μm in size were found inside the molybdenite rosettes.

Chemical composition of Au alloys

Backscattered electron (BSE) images of polished sections show an even distribution of elements in the grains. The major components are Au, Ag, and Cu (Table 7). Lamellae zones slightly enriched in Ag and depleted in Cu exist, whereas Au was evenly distributed. The EDS data indicate that the alloy has a composition of $(Cu,Ni,Zn)_3(Au, Ag)_2$, with variations from $(Cu, Ni, Zn)_{2.72}(Au, Ag)_{2.28}$ to $(Cu, Ni, Zn)_{2.99}(Au, Ag)_{2.01}$. Exsolution textures were not recognized in either BSE images or reflected light. Uniform compositions similar to the Kudryavy triple alloys, being homogeneous in reflected light and with uniform distribution of BSEs, have never been reported to our knowledge (Knight and Leitch 2001; Nekrasov et al. 2001; Spiridonov and Pletnev 2002).

Table 7 Results of EDS analyses of Cu–Au–Ag alloys from the Kudryavy volcano

No.	Fumarolic field	*T* (°C)	Element (wt%)					
			Ni	Cu	Zn	Ag	Au	Total
1	Main, tube	870		35.15		7.16	59.80	102.11
2				32.76		7.82	60.68	101.26
3				34.09		9.62	58.35	102.06
4[a]	Rhenium, tube	290		29.37		7.24	63.39	100.00
5[a]				28.38		9.81	61.81	100.00
6	Molybdenum	645		35.13		7.74	58.42	101.29
7	Dome	690	0.25	28.46	0.73	10.63	57.33	97.40
8			ND	34.04	0.50	7.66	60.70	102.88
9			0.41	32.62	0.52	6.72	59.50	99.78
10				30.67		10.25	57.08	98.41

Blank table entries were not analyzed
ND Below detection limit
[a]Normalized results

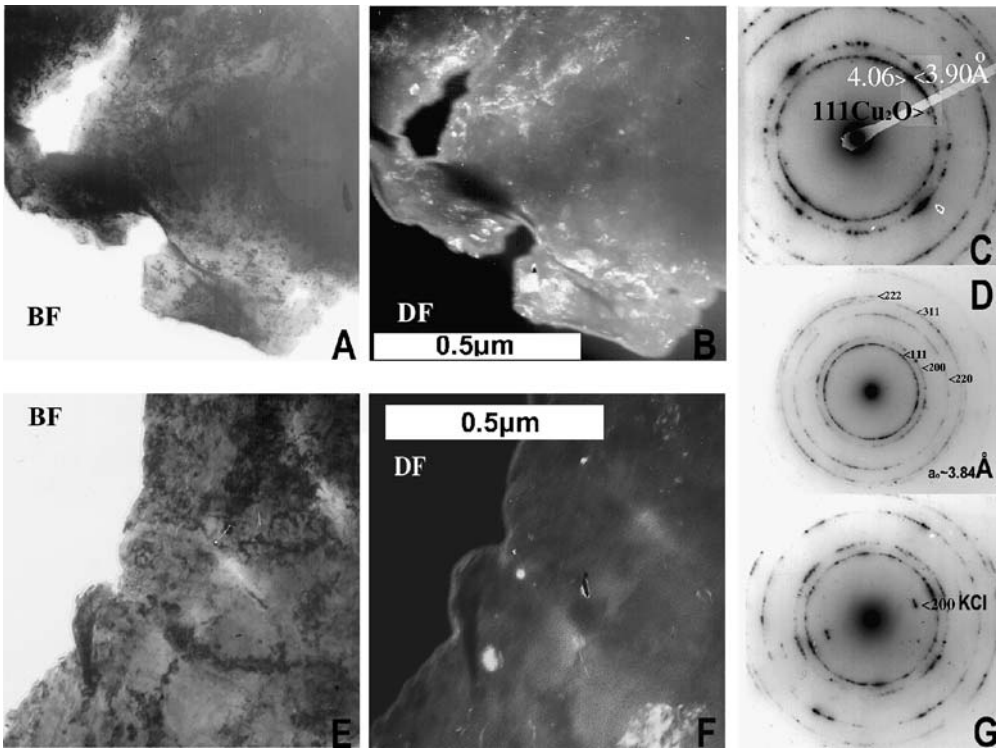

Fig. 12 TEM images of Cu–Au–Ag alloy. **a** Bright field image; **b** dark field image of 111 and 222 reflections of alloy foil, illustrated range of size of monocrystal solid solution grains (from less than 100 to 800 Å); **c** SAED pattern with reflections corresponding to Au, Ag phase (a_o ~4.06 Å) and cuprite Cu_2O; **d** SAED pattern of Cu–Au–Ag alloy with a_o approximately 3.84 Å; **e**, **f** bright and dark field image of alloy with inclusions of sylvite KCl (*bright white spots*) **g** SAED pattern with additional reflections of sylvite

TEM data

The study using a TEM showed nanometer-scale structural and compositional heterogeneity of the triple alloys (Fig. 12). The observed variations of the cell parameters confirmed that the disordered solid solution is not homogeneous and exists as a mixture of binary phases, including Cu–Au and Au–Ag ones. These phases are composed of monocrystal domains of solid solutions that range from tens to 800 Å and can be seen on the dark field image of 111 and 222 reflections (Fig. 12a,b). In the selected area electron diffraction (SAED) pattern, variations of ring reflection intensities and interplanar spacings correspond to a disordered cubic face-centered cell with a predominant parameter of a=3.84±0.06 Å (Fig. 12), which is characteristic of a binary Au–Cu alloy. Additional weak reflections observed near 111 and 222 ring reflections correspond to a=4.04–4.08 Å (Fig. 10d) and is typical of a binary Au–Ag alloy. We also recorded spot reflections corresponding to d=2.44 Å, and this probably belongs to cuprite Cu_2O (Fig. 12c).

No superlattice reflections typical of phases in the Cu–Au system were found. Some additional reflections were caused by sylvite and halite inclusions from tens to hundreds of angstroms in size (Fig. 12f,g).

Discussion

Based upon the presented data, transport by high-temperature low-density fluids with involvement of such complex anions as F, Cl, S, Br, and I allows for the migration and concentration of Au and a large group of coexisting metals such as Mo, W, Cr, Re, Pb, Zn, Cu, Ag, Ni, Bi, Cd, and In.

Mechanisms and forms of gold migration

Thermodynamic data show that Au, Ag, and Cu behave similarly in both hydrothermal solutions and in gas (Tkachenko et al. 1999; Akinfiev and Zotov 2001). All of these metals have extremely low vapor partial pressures as a pure phase, but their compounds with Cl are highly volatile. They can be transported in acidic conditions as simple chlorides such as Au_2Cl_{6gas} and Ag_3Cl_{3gas} and can be replaced by $[MeCl_2]^{1-}$ and $[MeCl_3]^{2-}$ complexes and such compounds such as [CuCl (H_2O)] with decreasing temperature (Tagirov et al. 1993; Mavrogenes et al. 2002; Williams-Jones et al. 2002). In terms of the Kudryavy fumarole gas compositions (near NNO redox buffer), where sulfur is present dominantly as SO_2, hydrosulfuric complexes do not play an essential role as a transporting agent in high-temperature fluids. The abundance of halite and sylvite in the precipitates and the high halogen content of gases suggest that chloride complexation plays an important role in noble metal transport. Metal precipitation was mainly governed by the temperature gradient and neutralization (dilution and decompression) of the initially more acidic (and denser) fluid during its ascent to the surface.

Kudryavy fluid occurs as a gas phase over the entire range of temperature (100–870°C) and pressure (close to atmospheric pressure 0.88−0.91 atm, Korzhinsky et al. 2004). Many transition metals in the products of supercritical fluid crystallization coexist in various valence states, from zero valence to a maximum valency. Such assemblages could be formed as a result of gas transport reactions, which are suggested to be the main mechanism of mineralization in the Kudryavy fumarolic system.

Native metals can precipitate according to gas transport reactions involving disproportionation reactions (Schafer 1961; Shmulovich and Churakov 1998), for example,

$$\underset{T_1(900)}{Au_{solid} + Cl_{2gas}} \rightarrow AuCl_{2gas} \rightarrow \underset{T_2(700)}{Au_{solid} + AuCl_{4gas}}.$$

Physicochemical mechanisms of gas transport reactions can be expressed as follows, in which any solid or liquid compound that reacts at high temperature with a gas to form gaseous products can be reversed by back reaction on cooling:

$$Fe_2O_{3solid} + 6HCl_{gas} \rightarrow 2FeCl_{3gas} + 3H_2O_{gas} \rightarrow Fe_2O_{3solid} + 6HCl_{gas}$$

or

$$2Al_{solid} + AlCl_{3gas} \rightarrow 3AlCl_{gas} \rightarrow 2Al_{solid} + AlCl_{3gas}.$$

The important features of such reactions are (1) they can facilitate gas transport of almost all metals, including Au and PGE, and their various compounds (oxides, salts, sulfides, and sulfosalts); (2) the crystallization temperature of metal compounds from gas is lower than that from a melt; (3) various gases such as halogens, hydrogen, oxygen, water, and chlorides can transport metals; (4) the amount of carrier matter is small in comparison to the amount of transported matter; and (5) they result in the formation of large idiomorphic crystals whose morphology may be controlled by parameters of the medium (a concept widely applied in the semiconductor and crystal growth industry). The main factor causing precipitation is a drop in temperature along the reaction path (Schafer 1961).

Zonation of precipitates

In general, zonation of the tube precipitates from Kudryavy is similar to those of other andesitic volcanoes (Symonds 1993), and general trends in tube zonation are in good agreement with the volatility of the main compounds (Churakov et al. 2000).

Results of ICP-MS analyses of the condensates involving the three different analytical schemes show a significant difference in Au (and some other elements) contents. The absence of Au on the filters shows that condensates are undersaturated in gold under normal conditions. Decreased Au content in method II likely is the result of a loss of volatile compounds during vaporization. The formation of volatile compounds probably is the main reason for metal losses during the preparation of the liquid condensates.

Gold abundance in the condensates does not exceed 2.5 ppb and is sufficiently lower than Au concentrations of natural and synthetic vapor inclusions, which were examined in recent studies employing laser ablation–inductively coupled plasma–mass spectrometry (LA-ICP-MS) (Ulrich et al. 1999; Simon et al. 2005). Au abundance in sublimates ranges from 1 up to 8 ppm, with increasing concentration corresponding to decrease in temperature. Most of the Au is concentrated in alloys, and triple alloys are found in high-temperature zones (500–870°C). Triple-alloy occurrences in the tubes coexist with oxide mineral assemblages, whereas in natural fumarolic sublimates, the triple alloys occur with Au-bearing Fe–Cu–Zn sulfides that encrust earlier-formed oxides. These Fe–Cu–Zn sulfides contain up to 5 ppm Au. The sulfide assemblage, including Cu-bearing pyrrhotite, Fe-rich wurtzite, chalcopyrite [or possibly high-temperature intermediate solid solution (ISS)], pyrite, and various Fe–Cu–Zn–Cd–In sulfides, plays the most important role in the concentration of invisible Au. Binary Au–Ag alloys and native Au mainly precipitated in the sulfide and oxychloride assemblages at temperatures below 400°C, as established for the rhenium field fumaroles.

High-temperature zones of mineralization are mainly composed of oxygen-bearing compounds: simple oxides, silicates, sulfates, molybdates, wolframates, and rhenates. The mineralogical observations suggest migration of VI group elements (Mo, W, Cr, and Re) as oxygen-bearing acids and oxychlorides, consistent with thermodynamic calculations (Churakov et al. 2000). Paragenesis of the triple Au alloy with high-temperature W, Mo, Re oxides, and Na–K chlorides allows for the possibility of Au transport as chloride and oxychloride complexes with alkali metals: $Na_2[AuCl_5]$–$Na_2[AuCl_3O]$–$Na_2[AuClO_2]$ etc. in terms of an analogy with $Na_2[WCl_8]$–$Na_2[WCl_6O]$–$Na_2[WCl_4O_2]$–$Na_2[WCl_2O_3]$. The decomposition of such compounds can result in the precipitation of Na–K chlorides, native elements, and oxides. The mineralogical evidence indicates a strong geochemical relationship of Au with halogens under high-temperature conditions. Under lower temperature conditions (<650°C), Au behavior is more closely connected to sulfur compounds whose evolution apparently is controlled by redox conditions. Our observations are in agreement with Gammons and Williams-Jones (1997), who described Au behavior in aqueous fluids of varying chemistry and concluded Au migration as $AuCl^{2-}$ and replacement by $AuHS^{2-}$ with cooling.

Most Mo precipitates from gas as molybdenite within a narrow temperature range of 720–650°C and is replaced by Zn, Cd, Fe, Re, Bi, and Pb sulfides within a wider temperature range. The remaining Mo remains volatile and crystallizes as oxide minerals.

Chlorides of Na and K predominate over sulfates in a high temperature range (>500°C) and are further distributed everywhere in subordinate amounts. Chlorides (more rarely iodides) of transition metals replace their sulfides with temperature decreases that are consistent with a higher volatility of their chlorides in comparison to sulfides.

Generally, the sequence of mineral precipitation from gas is controlled by the volatility of their gaseous species and depends on temperature, pressure, and concentration in the fluid. The weakly volatile species precipitate first, and the highly volatile compounds migrate to lower tempera-

ture zones. The volatilities of native metals are extremely low, so transport and deposition of native elements results from the disintegration of their more volatile compounds. The multicomponent composition of natural volcanic gases saturated with halogens and other complex ligands leads to the formation of a great number of volatile species for each element. In addition, the transition metals may form compounds in various oxidation states as a result of disproportionation reactions, and the deposition of mineral phases is accompanied by a formation of additional volatile compounds, which in turn decomposes at a lower temperature. This results in the formation of mineral assemblages of the same element with different valence states that conflicts with the phase rule. Coeval deposition of native Mo, ferrimolybdite, and molybdenite in a single temperature zone illustrates such an occurrence.

Occurrences of gold in minerals

Occurrences of native Au in volcanic sublimates are common, although direct measurement of the Au content of high-temperature volcanic gas condensates typically yields concentrations near the detection limit of modern analytical techniques (Taran et al. 2000). The occurrences of Au for the fumarolic precipitates from Tolbachik volcano have been described in detail (Vergasova et al. 1982; Karpov et al. 2001). High-fineness native Au- and Ag-bearing native Au occur as single-plate, needle, and hair-like crystals at temperatures of 180–320 and 400–625°C on different volcanic cones, whereas gas condensates only contain up to 0.087 ppb Au, with an average value of 0.016 ppb. The highest Au contents (Au 142.88 ppm) were found in the bulk sample of altered volcanic rocks with Cu-chloride mineralization. Na-, Al-, and Mg-fluoride mineralization is also rich in Au (Au 100.8 ppm).

On Colima volcano (Taran et al. 2000), trigonal and pentagonal plates of native Au in quartz tube sublimates precipitated within the narrow temperature range of 550–600°C in association with V-rich Na–K sulfate. The Colima gas condensates are characterized by low Au (<0.5 ppb), but the sublimates precipitated from this gas are extremely enriched with up to 58 ppm Au, corresponding to ore-grade mineralization. The highest Au abundance was measured in volcanic gas condensates (Au 32 ppb) from the rhyolitic Satsuma Iwojima volcano (Hedenquist et al. 1994). Gases from the basaltic Momotombo and Etna volcanoes are also enriched with Au (up to 24 ppb). Fulignati and Sbrana (1998) reported the presence of native Au and native Te in the sublimates of the high-temperature silica zone of a fumarole with a temperature range of 170–540°C near the rim of La Fossa volcano (Vulcano, Italy). Some particles are pure native Au, while others contain significant amounts of Cu and Ag.

Cu–Au–Ag triple alloys are rare in ores. Binary Au–Cu alloys are common in deposits associated with mafic and ultramafic intrusions and related placers. Minerals in the Au–Cu and Au–Cu–Pd systems are characteristic of mineralization in serpentinized dunite, peridotite, rodingite, komatiite, and layered mafic complexes (Knight and Leitch 2001; Murzin et al. 1987; Ramdohr 1982; Spiridonov and Pletnev 2002; Sluzhenikin and Mokhov 2002). A number of Cu–Au, Au–Pt–Cu, Au–Pd–Cu, and Au–Ag–Cu alloys occur in the Pt-bearing placers of the Konder alkaline ultramafic massif (Nekrasov et al. 2001). The alloys of the Cu–Au–Ag system commonly display multiphase exsolution textures, which are interpreted as examples of post-crystalization transformations (Knight and Leitch 2001). Three compositional fields of disordered solid solutions corresponds to Cu_3Au, CuAu, and $CuAu_3$ with a face-centered cubic lattice known in synthetic and natural systems (Novgorodova 1983; Knight and Leitch 2001). Lamellar and zonal structures of triple alloys with lamellae thicknesses of 1–2 μm in association with garnet and pyroxene were studied by Novgorodova (1983) in the rodingite from the Zolotaya Gora (Urals). She showed that $Cu_3(Au,Ag)_2$ compositions characterize the mixtures of the two phases and described epitaxial intergrowths on 111 of two lamellar phases—native Au and auricupride with incomplete ordering. The chemical composition of the Au–Cu alloys falls mainly in the Ag-poor part of the Au–Ag–Cu ternary diagram, and in turn, the composition of the Au–Ag alloys is depleted in copper. The triple alloys from Kudryavy volcano demonstrate that such lamellar morphology can be a primary texture of these high-temperature compounds and is not necessarily the result of superimposed transformations.

At Kudryavy, triple alloys are associated with high-temperature mineralization and likely from supercritical aqueous fluids. Precipitation from a gas phase also was suggested for similar lamellar Au in the Pavlovsk coal deposit (Russian Far East) (Seredin 2004) and for a Cu–Au–Ag–Zn alloy from a lunar regolith multimetal mineralization (Bogatikov et al. 2001).

Crystal growth mechanism

The high idiomorphism of the sublimate minerals reflects their free growth in a gaseous environment. Aggregates of separate plates of triple alloys are frequently twisted, while binary Au–Ag alloys occur commonly as simple platelets. The spiral growth of triple alloys can be caused by both metal impurities and inclusions of K and Na chlorides. Experimental data on the growth of platy crystals from a gas indicate that impurities initiate an anisotropic growth of lamellar-, banded-, skeletal-, and dendrite-like crystals (Givargizov 1977; Symonds 1993). A key factor in the formation of anisotropic crystals is a domain structure with surfactants such as halides (Zheng et al. 2004). Heteroepitaxial growth of native metals (Au, Ag, and Cu) on a surface of KCl crystals has also been experimentally demonstrated (Vlasov and Kanevskij 2004).

The widespread occurrence of platy, needle-shaped, and skeletal forms among fumarole minerals is consistent with fast growth from saturated fluids. Growth of platy crystals begins with whisker formation, and then further growth occurs by a vapor–liquid–solid mechanism with aggrega-

tion of nano-sized clusters both in cavities and directly in the gas flow (Givargizov 1977). The domain structure of the triple alloys probably indicates their initial crystallization as clusters of binary Au–Ag and Au–Cu alloys followed by epitaxial accretion. The direct crystallization from gas seems obvious in the case of native Ag and native Al growth on the clean surface of a silica tube. On the other hand, arched and twirled whiskers and ontolites of chlorides and anhydrite occur from salt melts by the vapor–liquid–solid mechanism.

Detailed observations of sublimate mineral surfaces frequently reveal fine nano-scale cluster structures expressed by a close intergrowth of separate plates, needles, spheres, and irregular-shaped particles depending on the symmetry of the crystals. Thus, framboidal galena is formed as a result of the intergrowth of numerous microframboids (Fig. 9g); skeletal crystals of K-perrhenate consist of separate skeletal blocks (Fig. 11d), and molybdenite and rheniite crystals are composed of lamellae with thicknesses of less than 0.1 μm. Cluster structures of sublimate minerals at the scale of electronic microscope observation has been noted by previous researchers (Shmulovich and Churakov 1998). Wide variations of both cationic compositions of the abundant minerals (Pb–Bi sulfosalts, Fe–Zn–Cd sulfide, Cu–Fe–Sn–In sulfides, etc.) and anionic compositions (wolframates–molybdates, spinels, complex sulfates, and sulfochlorides) may also be caused by cluster growth. Precipitates in the low-temperature zones of tubes are enriched in some metals (Mo, Re, Au, and others) and represent the mix of dispersed clusters of various nonstoichiometric compositions but not monomineralic crystals.

Conclusions

Gas transport reactions can precipitate Au-bearing mineral assemblages from a slightly reduced (near NNO buffer), high-temperature, low-density fluid that is unsaturated with respect to Au (Gammons and Williams-Jones 1997). Low Au contents in gases (approximately 1–2 ppb in condensates) are enough for the formation of Au minerals such as Cu–Au–Ag triple alloys at temperatures up to 850°C. The formation of triple alloys seems to be related to the decomposition of volatile halide complexes with decreases in temperature.

The magmatic vapor phase remains capable of transporting Au upon cooling. The lower-temperature (<650°C) mineral associations are more enriched in Au, but Au occurs mainly as a constituent in sulfide minerals. Binary Au–Ag alloys and native Au as well as sulfide and oxychloride assemblages rich in Au, up to 8 ppm, precipitate at temperatures lower than 400°C.

Crystallization from a gas phase and formation of triple alloys likely occurred in ore deposits, and textural evidence of such should be examined. The lamellar structure of triple alloys is the primary feature occurring from fast growth from gas unsaturated in alloy components.

Besides Au, native Pt, Al, Si, Ti, Mo, Cr, Sn, Cu, Ag, and Se occur in the sublimate assemblages. The gas transport mechanism and the nano-scale phase formation allow coexistence of the reduced and oxidized phases of the transition metals. In the Kudryavy case, formation of native metals does not necessarily involve highly reduced or hydrogen-rich fluids. Such nonequilibrium associations with coexisting various valence states are characteristic of high-temperature stages where the hydrothermal fluids exist as a gas phase, and mineral assemblages are precipitated as a result of gas transport reactions. Multiple superimposed hydrothermal processes may mask evidence of high-temperature gas transport in ancient deposits, but relicts can be identified in the mineral paragenesis.

The geodynamical position of Kudryavy volcano and geochemical characteristics of its sublimate mineral assemblages have much in common with typical Cu±Mo±Au porphyry mineralization. Indeed, the majority of giant gold-rich porphyry deposits occur in similar settings around the "ring of fire" along the boundary of the Pacific plate. Thus, the geochemical processes and mineralogical characteristics identified in this study may have broad applicability in understanding ore deposits worldwide, both ancient and modern.

Acknowledgements This study was supported by the Russian Foundation for Basic Research, project no. 04-05-64946, and the Department of Science on Earth, Russian Academy of Sciences ("Nanoparticles in nature" program). The authors thank M. Kuznetzova and A. Kerzin for valuable assistance and analytical support. We are grateful for constructive comments by I. Vikentyev, L. Wardell, J. Mungall, and J. Hanley on an early version of the manuscript. Thorough reviews by S.F. Simmons and N.C. White are acknowledged. The final version of the manuscript was significantly improved by the thoughtful editing of L. Meinert.

References

Akinfiev NN, Zotov AV (2001) Thermodynamic description of chloride, hydrosulfide, and hydroxo complexes of Ag(I), Cu(I), and Au(I) at temperatures of 25–500°C and pressures of 1–2000 bar. Geochem Int 39:990–1006

Bindeman IN (1997) Recurrent magma and cumulate mixing as a mechanism of the cyclic evolution of Baranskogo volcano, Iturup, Kuril Islands. Geochem Int 35:329

Bogatikov OA, Gorshkov AI, Mokhov AV, Ashikhmina NA, Magazina LO (2001) The first finding of native molybdenum, silver sulfide, and iron–tin alloy in the lunar regolith. Geochem Int 39:604–609

Botcharnikov RE, Shmulovich KI, Tkachenko SI, Korzhinsky MA, Rybin AV (2003) Hydrogen isotope geochemistry and heat balance of a fumarolic system: Kudriavy volcano, Kuriles. J Volcanol Geotherm Res 124:45–66

Chaplygin IV, Mozgova NN, Bryzgalov IA, Mokhov AV (2004) Cadmoindite $CdIn_2S_4$, a new mineral from Kudryavy volcano, Iturup Isle, Kurile Islands. Zap Vseross Mineral Obsestva 133 (4):21–27 (in Russian)

Churakov SV, Tkachenko SI, Korzhinskii MA, Bocharnikov RE, Shmulovich KI (2000) Evolution of composition of high-temperature fumarolic gases from Kudryavy volcano, Iturup, Kurile Islands: the thermodynamic modeling. Geochem Int 38:436–452

Cygan GL, Candela PA (1995) Preliminary study of gold partitioning among pyrrhotite, pyrite, magnetite, and chalcopyrite in gold-saturated chloride solutions at 600 to 700°C, 140 MPa (1400 bars). In: Thompson JFH (ed) Magmas, fluids, and ore deposits, short course, vol 23. Mineralogical Association of Canada, Ottawa, pp 129–137

Distler VV, Yudovskaya MA, Znamenskii VS, Chaplygin IV (2002) Platinum group elements in modern fumaroles of the Kudryavy volcano, Iturup Island, Kurile Island Arc. Dokl Earth Sci 387:975–979

Ermakov VA, Steinberg GS (1998) Kudryavy volcano and evolution of the Medvezhya caldera (Iturup Isle, Kurile Islands). Vulcanol Seism 12:12–24 (in Russian)

Ermakov VA, Znamensky VS, Steinberg GS (2001) The petrology of the volcano-caldera Medvezhya (Kurile Islands). Izv RAEN, Earth Sci Sect 6:97–118

Fischer TP, Giggenbach WF, Sano Y, Williams SN (1998) Fluxes and sources of volatiles discharged from Kudryavy, a subduction zone volcano, Kurile Islands. Earth Planet Sci Lett 160:81–96

Fulignati P, Sbrana A (1998) Presence of native gold and tellurium in the active high-sulfidation hydrothermal system of the La Fossa volcano (Vulcano, Italy). J Volcanol Geotherm Res 86:187–198

Gammons CH, Williams-Jones AE (1997) Chemical mobility of gold in the porphyry-epithermal environment. Econ Geol 92:45–59

Giggenbach WF (1975) A simple method for the collection and analysis of volcanic gas samples. Bull Volcano 39:132–145

Givargizov EI (1977) Growth of crystal whiskers and lamellas from vapor. Nauka, Moscow (in Russian)

Hedenquist JW, Aoki M, Shinohara H (1994) Flux of volatile and ore-forming metals from the magmatic-hydrothermal system of Satsuma Iwojima volcano. Geology 22:585–588

Karpov GA, Vergasova LP, Kardanova OF (2001) Gold on products of post-magmatic processes in the transitional zone continent-ocean (Kamchatka). Geodynamic, magmatism and mineragenesis of the Northern Pacific continental margin. Vladivostok 215–218

Kesler SE, Chryssoulis SL, Simon G (2002) Gold in porphyry copper deposits: its abundance and fate. Ore Geol Rev 21:103–124

Knight J, Leitch CHB (2001) Phase relations in the system Au–Cu–Ag at low temperatures, based on natural assemblages. Can Mineral 39:889–906

Korzhinsky MA, Tkachenko SI, Bulgakov RF, Shmulovich KL (1996) Condensate compositions and native metals in sublimates of high-temperature gas streams of Kudryavy Volcano, Iturup Island, Kuril Islands. Geochem Int 36:1175–1182

Korzhinsky MA, Bocharnikov RE, Tkachenko SI, Zhdanov NN, Steinberg GS (2004) Variations of the composition of high-temperature fumarole gas on the Kudryavy volcano, Iturup Island, South Kuriles. Experimental mineralogy: some results on the century's frontier. Nauka, Moscow, pp 127–148 (in Russian)

Kovalenker VA, Laputina IP, Znamensky VS, Zotov IA (1993) Indium mineralization of the Great Kuril Arc. Geol Ore Depos 35:547–552

Kovtunovich PY, Safronov AD, Udodov VV, Rasshepkina EV (2000) State geological map of Russian Federation 1:200000, 2nd edn. Kuriles series

Le Guern F, Bernard A (1982) A new method for sampling and analyzing sublimates. Application to Merapi volcano, Java. J Volcanol Geotherm Res 12:133–146

Mavrogenes JA, Berry AJ, Newville M, Sutton SR (2002) Copper speciation in vapor-phase fluid inclusions from the Mole Granite, Australia. Am Mineral 87:1360–1364

Meeker K, Chuan R, Kyle PR, Palais J (1991) Emission of elemental gold particles from Mount Erebus, Ross Island, Antarctica. Geophys Res Lett 18:1405–1408

Murzin VV, Kudryavtsev VI, Berzon HO, Sustavov SG (1987) Cuprous gold in zones of rodingite. Geol Ore Depos 29:96–99

Nekrasov IY, Ivanov VV, Lennikov AM, Sapin VI, Safronov PP, Oktyabrskii RA (2001) Rare natural polycomponent alloys based on gold and copper from a platinum placer in the Konder alkaline-ultrabasic massif, southeastern Aldan Shield, Russia. Geol Ore Depos 43:406–418

Novgorodova MI (1983) Native metals in hydrothermal ore. Nauka, Moscow (in Russian)

Ramdohr P (1982) The ore minerals and their intergrowths. Pergamon, New York

Schafer H (1961) Chemische transportreaktionen. Verlag Chemie, Weinheim (Russian version: Mir, Moscow)

Seedorff E, Einaudi MT (2004) Henderson porphyry molybdenum system, Colorado: II. Decoupling of introduction and deposition of metals during geochemical evolution of hydrothermal fluids. Econ Geol 99:39–73

Seredin VV (2004) The Au-PGE mineralization at the Pavlovsk brown coal deposit, Primorye. Geol Ore Depos 46:36–59

Shmulovich KI, Churakov SV (1998) Natural fluid phases at high temperatures and low pressures. J Geochem Explor 62:183–191

Sillitoe RH (2000) Gold-rich porphyry copper deposits: descriptive and genetic models and their role in exploration and discovery. In: Hagemann SG, Brown PE (eds) Gold in 2000. Rev Econ Geol 13:315–345

Simon AC, Frank MR, Pettke T, Candela PA, Piccoli PM, Heinrich CA (2005) Gold partitioning in melt–vapor–brine systems. Geochim Cosmochim Acta 69:3321–3335

Sluzhenikin SF, Mokhov AV (2002) Gold and silver in deposits of Norilsk region. Geology, genesis and questions of development of complex noble metal deposits. IGEM RAS, Moscow, pp 326–330 (in Russian)

Spiridonov EM, Pletnev PA (2002) The Zolotaya Gora cuprous gold deposit. Nauchny Mir, Moscow (in Russian)

Symonds R (1993) Scanning electron microscope observations of sublimates from Merapi volcano, Indonesia. Geochem J 26:337–350

Tagirov VK, Makarov VA, Brukvin VA (1993) Vapor composition and pressure over chlorides of silver and gold. Metalli 5:67–71 (in Russian)

Taran YA, Hedenquist JF, Korzhinsky MA, Tkachenko SI, Shmulovich KI (1995) Geochemistry of magmatic gases from Kudryavy volcano, Iturup, Kuril islands. Geochim Cosmochim Acta 59:1749–1761

Taran Y, Bernard A, Gavilanes JC, Africano F (2000) Native gold in mineral precipitates from high-temperature volcanic gases of Colima volcano, Mexico. Appl Geochem 15:337–346

Tessalina S, Yudovskaya M, Capmas F, Birck JL, Distler V, Chaplygin I, Allègre CJ (2005) Unique rhenium enrichment in the Kudryavy volcano, Kurile Islands: evidences from Re–Os isotopic studies. In: Goldschmidt conference abstracts 2005

Tkachenko SI, Porter RP, Korzhinskii MA, van Bergen MD, Shmulovich KI, Shteinberg GS (1999) Mineral- and ore-forming processes in high-temperature fumarolic gases at Kudryavy volcano, Iturup Island, Kuril Archipelago. Geochem Int 37:355–366

Tolstykh ML, Naumov VB, Kononkova NN (1997) Three types of melt in the basaltic andesite from the Medvezhya Caldera, Iturup, Southern Kurile Islands. Geochem Int 35:339–346

Ulrich T, Gunther D, Heinrich CA (1999) Gold concentrations of magmatic brines and the metal budget of porphyry copper deposits. Nature 399:676–679

Vergasova LP, Naboko SI, Serafimova EK, Starova GL, Filatov SK (1982) Exhalational native gold. Dokl Trans Acad Sci USSR 264:201–203 (in Russian)

Vlasov VP, Kanevskij VM (2004) A role of silver halide sublayers at gold and silver epitaxy on a surface (010) of K chlorides. In: Abstracts of XX Russian conference on electron microscopy, Chernogolovka, 1–4 June 2004, p 23 (in Russian)

Williams-Jones AE, Migdisov AA, Archibald SM, Xiao ZF (2002) Vapor-transport of ore metals. In: Hellmann R, Wood SA (eds) Water–rock interaction: a tribute to David A. Crerar. Geochemical Society Special Publication 7, pp 279–305

Zheng X, Zhu L, Wang X, Yan A, Xie Y (2004) A simple mixed surfactant route for the preparation of noble metal dendrites. J Cryst Growth 260:255–262

Znamensky VS, Laputina IP, Taran YA, Yakushev AI (1993) Ore deposition from the high-temperature gas stream of the Kudryavy volcano, Iturup island, Kurile Islands. Dokl Earth Sci 333:227–230

Znamensky VS, Korzhinsky MA, Steinberg GS, Tkachenko SI, Yakushev AI, Laputina IP, Bryzgalov IA, Samotoin ND, Magazina LO, Kuzmina OV, Organova NI, Rassulov VA, Chaplygin IV (2005) Rheniite ReS_2, a natural rhenium bisulfide from fumaroles of Kudryavy volcano, Iturup Isl., Kurile Islands. Zap Ross Mineral Obsestva 134(5):32–40